Covariant confinement model for the calculation of radial excitations of the pion

L. S. Celenza, Bo Huang, and C. M. Shakin*
Department of Physics and Center for Nuclear Theory, Brooklyn College of the City University of New York, Brooklyn, New York 11210
(Received 29 July 1998)

We describe the mixing of $q\bar{q}$ pseudoscalar states with longitudinal $q\bar{q}$ axial-vector states, making use of a relativistic quark model that includes a model of confinement. (In the absence of the confinement model, our model reduces to the Nambu–Jona-Lasinio model.) In addition to the pion, we find $J^P=0^-$ states at 1.18, 1.36, 1.47, 1.63, and 1.68 GeV. The first two of these states are in the region of the $\pi(1300)$ that is assigned a mass of 1300 ± 100 MeV and a width of 200–600 MeV in the data tables. We provide values of the coupled-channel $q\bar{q}$ T matrix, as well as the mixing angle, which is energy-dependent in our analysis. In addition, we describe a model of confinement for longitudinal axial-vector $q\bar{q}$ states that is used in the calculation of vacuum polarization diagrams. (That analysis supplements our previous study of confinement in the case of pseudoscalar mesons.) We show that our confinement model may be made covariant. We use the covariant model to calculate the decay of the various states, π', to the $\pi+\rho$ and $\pi+\sigma$ channels at one-loop order. At one-loop order, it is found that only the nodeless state at 1.18 GeV and the state at 1.36 GeV have significant widths for $\pi'\to\pi+\sigma$. These states have somewhat larger widths for the decay $\pi'\to\pi+\rho$, leading to $\Gamma_{\rm tot}=0.368$ GeV for the state at 1.18 GeV and 0.150 GeV for the state at 1.36 GeV. We note that the state 1.18 GeV is a mixed pseudoscalar–axial-vector state, while the state at 1.36 GeV is the $\pi(2S)$ state to a good approximation, since it has a very small admixture of axial-vector components. There is information concerning the decay $\pi'\to\pi+(\pi+\pi)_{L=0}$ that is extracted from experimental data for three-body final states. Our (nodeless) state at 1.18 GeV has the correct energy and width to fit that data. However, our widths for $\pi'\to\pi+(\pi+\pi)_{L=1}$ are larger than those for $\pi'\to\pi+(\pi+\pi)_{L=0}$. That suggests that final-state interactions are probably quite important in understanding the branching ratios for π' decays to states of three pions. Our results also suggest that, if we were to study the $\pi(1300)$, and include final-state interactions, it is necessary to include both the 1.18 GeV and the 1.36 GeV states in the analysis. (On the other hand, since the 1.36 GeV state is a $2S$ state, it may be only weakly excited in the reactions used to generate final states of three pions.) [S0556-2813(99)05802-1]

PACS number(s): 24.85.+p, 12.39.−x, 14.40.Aq

I. INTRODUCTION

In a series of papers, we have been developing an effective field theory for quarks based upon the Nambu–Jona-Lasino (NJL) model [1], supplemented with a relativistic model of confinement [2–6]. In previous work we have studied singlet-octet mixing for scalar-isoscalar mesons [3], η-η' mixing and ϕ-ω mixing [4]. We have also studied the spectrum of light and heavy mesons, including charmonium and bottomonium [5]. In the present work we extend our considerations to the mixing between pseudoscalar states and longitudinal axial-vector states, a phenomenon that is usually called ''π-a_1 mixing.'' A novel feature of the present study is that we are able to study this mixing in the energy region $0\leqslant P^2\leqslant 3.0\,\mathrm{GeV}^2$. (The usual discussion is limited to low energies, in the absence of a model of confinement.) We are particularly interested in the region where one finds the $\pi(1300)$, since little is known concerning that resonance. (In the data tables one finds that the energy is 1300 ± 100 MeV, while the width is given as 200–600 MeV [7].)

We find it useful to divide our analysis in two parts. For the low-energy domain. $P^2\leqslant 0.1\,\mathrm{GeV}^2$, we neglect confinement, while for $0.1\,\mathrm{GeV}^2\leqslant P^2\leqslant 3.0\,\mathrm{GeV}^2$ we include our confinement model. That is done, since pion properties are very sensitive to violation of chiral symmetry, and while our Lagrangian respects chiral symmetry in the absence of current quark masses, our approximations, in the case of Minkowski-space calculations, violate chiral symmetry to some degree. (A Euclidean-space analysis was presented in Ref. [6], where we showed that chiral symmetry may be maintained in the calculation, and that the Goldstone theorem is satisfied.)

In Sec. II of this work we review our treatment of the vacuum polarization diagrams that play an important role in the NJL model. We also show how the calculation of the polarization diagrams is modified when we include our confinement model. The confinement model eliminates cuts in the P^2 plane, that would appear when the quark and antiquark both go on mass shell. Therefore, the vacuum polarization integrals, $J(P^2)$, are real, if we do not take into account decay into open channels, such as $\pi+\gamma$, $\rho+\pi$, etc.

In Sec. III, we study the $q\bar{q}$ T matrix that describes the coupling of the $q\bar{q}$ pseudoscalar channel to the longitudinal component of the $q\bar{q}$ axial-vector channel. Singularities of the T matrix correspond to resonant states of the system.

In Sec. IV, we present the results of our analysis for $P^2\leqslant 0.10\,\mathrm{GeV}^2$, while in Sec. V, we present results for the region $0.10\,\mathrm{GeV}^2\leqslant P^2\leqslant 3.0\,\mathrm{GeV}^2$. It is the ability to treat the intermediate-energy region that is a novel feature of our approach. The low-energy region, described in Sec. IV, may be treated by standard methods. However, we include a discus-

*Electronic address: CASBC@CUNYVM.CUNY.EDU

sion of that region for the sake of completeness. In Sec. V we present our results for the spectrum of the mixed π-a_1 states and in Sec. VI we begin a discussion of a *covariant* model of confinement, which is needed for the calculation of the decay of the mixed π-a_1 states to the channels $\pi+\rho$ and $\pi+\sigma$. In Sec. VI we describe a vertex function of the confining interaction for pseudoscalar states, while Sec. VII contains a corresponding discussion for scalar states. The more complicated confinement vertex function for vector states is taken up in Sec. VIII and in the Appendix.

In Sec. IX we describe a covariant calculation of the decay amplitude $\pi' \to \pi+\rho$ where π' is any of the states found in this work, other than the $\pi(138)$. Section X contains a similar discussion of the decay amplitude for $\pi' \to \pi+\sigma$. In Sec. XI we describe the calculation of the decay widths for each of the states considered here. Finally, Sec. XII describes some aspects of the experimental data obtained from the study of the three-pion final states, as well as some further discussion.

II. VACUUM-POLARIZATION FUNCTIONS AND A MODEL OF CONFINEMENT

For the purposes of this work, we consider the Lagrangian with SU(2)-flavor symmetry [1]

$$\mathcal{L}=\overline{q}(i\partial-m^0)q+\frac{G_S}{2}[(\overline{q}q)^2+(\overline{q}i\gamma_5\vec{\tau}q)^2] - \frac{G_V}{2}[(\overline{q}\gamma^\mu\vec{\tau}q)^2+(\overline{q}\gamma^\mu\gamma_5\vec{\tau}q)^2]+\mathcal{L}_{\rm conf}, \quad (2.1)$$

where $m^0=\mathrm{diag}(m_u^0,m_d^0)$. We use Lorentz-vector confinement with

$$\mathcal{L}_{\rm conf}(x)=\int d^4y\,\overline{q}(x)\gamma^\mu q(x)V^c(x-y)\overline{q}(y)\gamma_\mu q(y). \quad (2.2)$$

Here, $V^C(r)=\kappa r\exp(-\mu r)$, where κ is the ''string tension'' and μ is a small parameter introduced to soften the singularities of the Fourier transform of $V^C(r)$. (If the parameter μ is small enough, the potential is essentially linear over the range of interaction considered.) We find

$$V^C(\vec{k}-\vec{k}')=-8\pi\kappa\left[\frac{1}{[(\vec{k}-\vec{k}')^2+\mu^2]^2}-\frac{4\mu^2}{[(\vec{k}-\vec{k}')^2+\mu^2]^3}\right], \quad (2.3)$$

in the case that we neglect energy transfer via the confining field. In this work we have taken $\mu=0.020\,\mathrm{GeV}$. [This model may be made covariant by expressing V^C in terms of the square of the difference of two four-vectors, $(k_c-k_c')^2$, that reduces to $-(\vec{k}-\vec{k}')^2$ in the meson rest frame, so that Eq. (2.3) is obtained.]

We begin our analysis by defining the polarization integrals

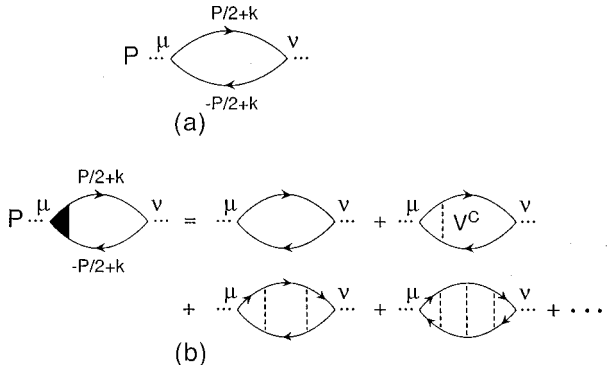

FIG. 1. (a) The diagram shows the basic vacuum polarization diagram of the NJL model in the absence of a confinement model. (b) The diagram serves to define the tensor $J^{\mu\nu}(P)$ in the presence of a confinement vertex, represented by the shaded triangular area (see Fig. 2). The right-hand side of the figure shows a perturbation expansion for $J^{\mu\nu}(P)$.

$$-i\hat{J}^{PP}(P)=(-1)n_cn_f\mathrm{Tr}\int\frac{d^4k}{(2\pi)^4} \times[i\gamma_5 iS(P/2+k)i\gamma_5 iS(-P/2+k)], \quad (2.4)$$

$$-i\hat{J}_\mu^{PA}(P)=(-1)n_cn_f\mathrm{Tr}\int\frac{d^4k}{(2\pi)^4} \times[iS(P/2+k)i\gamma_5 iS(-P/2+k)\gamma_\mu\gamma_5], \quad (2.5)$$

$$-i\hat{J}_\mu^{AP}(P)=(-1)n_cn_f\mathrm{Tr}\int\frac{d^4k}{(2\pi)^4} \times[iS(P/2+k)\gamma_\mu\gamma_5 iS(-P/2+k)i\gamma_5], \quad (2.6)$$

and

$$-i\hat{J}_{\mu\nu}^{AA}(P)=(-1)n_cn_f\mathrm{Tr}\int\frac{d^4k}{(2\pi)^4} \times[iS(P/2+k)\gamma_\mu\gamma_5 iS(-P/2+k)\gamma_\nu\gamma_5]. \quad (2.7)$$

(See Fig. 1.) Here $S(P)=[\not{P}-m+i\epsilon]^{-1}$, with m being the constituent quark mass. Further, the number of flavors is $n_f=2$ and the number of colors is $n_c=3$. We also define

$$J_\mu^{PA}(P)=iJ^{PA}(P^2)\frac{P_\mu}{\sqrt{P^2}}, \quad (2.8)$$

$$J_\mu^{AP}(P)=iJ^{AP}(P^2)\frac{P_\mu}{\sqrt{P^2}}, \quad (2.9)$$

and

$$J_{\mu\nu}^{AA}(P)=-\tilde{g}_{\mu\nu}(P)J_T^{AA}(P^2)-\frac{P_\mu P_\nu}{P^2}J_L^{AA}(P^2), \quad (2.10)$$

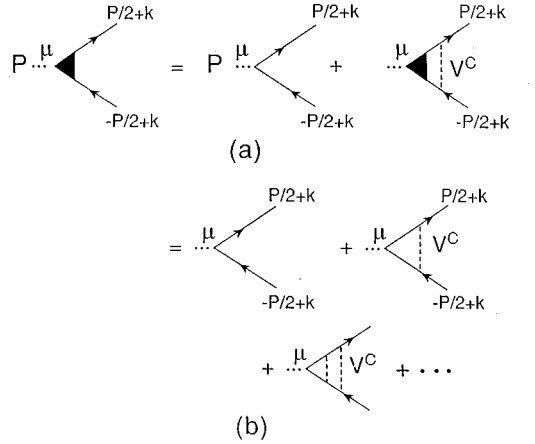

FIG. 2. (a) The equation for the vertex operators, $\Gamma^{\mu}(P,k)$ is shown. The vertex is represented by the filled triangular area and the dashed line represents the confining interaction. (b) A perturbative expansion is shown for the equation in (a). We see that the vertex serves to sum a ''ladder'' of confining interactions.

with $\tilde{g}_{\mu\nu}=g_{\mu\nu}-P_{\mu}P_{\nu}/P^2$. Note also that $J^{AP}(P^2)=-J^{PA}(P^2)$ and $P_{\mu}\tilde{g}^{\mu\nu}=\tilde{g}^{\mu\nu}P_{\nu}=0$.

The separation of transverse and longitudinal parts of the tensor $J^{AA}_{\mu\nu}(P)$ is appropriate, since the transverse part may be treated separately. Thus, only $J^{PP}(P^2)$, $J^{PA}(P^2)$, $J^{AP}(P^2)$ and $J^{AA}_{L}(P^2)$ will appear in the coupled equations that describe π-a_1 mixing. (We use the designation ''π-a_1 mixing'' as a simple phrase describing the phenomenon considered here.) Without a model of confinement, the polarization integrals will have unphysical cuts starting at $P^2=4m^2$ that correspond to the quark and antiquark going on their (positive) mass shells. That feature is eliminated by our confinement model.

For this calculation, the confining interaction $V^C(\vec{k}-\vec{k}')$ is used to define two vertex functions. (See Fig. 2.) Our treatment of these functions has its origin in the method used to calculate the vacuum polarization integrals. These are calculated by using the relation

$$S(P)=\frac{m}{E(\vec{P})}\left[\frac{\Lambda^{(+)}(\vec{P})}{P^0-E(\vec{P})+i\epsilon}-\frac{\Lambda^{(-)}(-\vec{P})}{P^0+E(\vec{P})-i\epsilon}\right] \tag{2.11}$$

for each propagator in Eqs. (2.4)–(2.7) and then performing the integral in the complex k^0 plane.

Let us first consider $J^{PP}(P^2)$, modified to include the confining vertex $i\overline{\Gamma}_5(P,k)$, which has a Dirac matrix structure,

$$-iJ^{PP}(P)=(-1)n_c n_f \,\mathrm{Tr}\int\frac{d^4k}{(2\pi)^4}[i\gamma_5 iS(P/2+k)\times i\overline{\Gamma}_5(P,k)iS(-P/2+k)]. \tag{2.12}$$

Use of Eq. (2.11) in Eq. (2.12), with $\vec{P}=0$, shows that only the elements $\Lambda^{(+)}(\vec{k})\overline{\Gamma}_5(P,k)\Lambda^{(-)}(-\vec{k})$ and $\Lambda^{(-)}(-\vec{k})\overline{\Gamma}_5(P,k)\Lambda^{(+)}(\vec{k})$ appear. Therefore, when $\vec{P}=0$, it is useful to define $\Gamma_5^{+-}(P,k)$,

$$\Lambda^{(+)}(\vec{k})\overline{\Gamma}_5(P,k)\Lambda^{(-)}(-\vec{k})=\Gamma_5^{+-}(P,k)\Lambda^{(+)}(\overline{k})\times\gamma_5\Lambda^{(-)}(-\vec{k}), \tag{2.13}$$

and $\Gamma_5^{-+}(P,k)$

$$\Lambda^{(-)}(-\vec{k})\overline{\Gamma}_5(P,k)\Lambda^{(+)}(\vec{k})=\Gamma_5^{-+}(P,k)\Lambda^{(-)}(-\vec{k})\times\gamma_5\Lambda^{(+)}(\vec{k}), \tag{2.14}$$

where $\Gamma_5^{+-}(P,k)$ and $\Gamma_5^{-+}(P,k)$ are ordinary functions with no Dirac matrix structure.

We may obtain equations for $\Gamma_5^{+-}(P,k)$ and $\Gamma_5^{-+}(P,k)$ starting with the equation for the matrix $\overline{\Gamma}_5(P,k)$,

$$\overline{\Gamma}_5(P,k)=\gamma_5-i\int\frac{d^4k'}{(2\pi)^4}[\gamma^{\rho}S(P/2+\vec{k}')\overline{\Gamma}_5(P,k')\times S(-P/2+k')\gamma_{\rho}V^C(\vec{k}-\vec{k}')]. \tag{2.15}$$

We proceed by multiplying this equation by $\gamma_5\Lambda^{(+)}(\vec{k})$ on the left, and by $\Lambda^{(-)}(-\vec{k})$ on the right, and then taking the trace. We find that if we neglect coupling between Γ_5^{+-} and Γ_5^{-+}, we have (for $\vec{P}=0$)

$$\Gamma_5^{+-}(P^0,|\vec{k}|)=1-\int\frac{d^3k'}{(2\pi)^3}\left[\frac{m^2-2E(\vec{k})E(\vec{k}')}{E(\vec{k})E(\vec{k}')}\right]\times\frac{\Gamma_5^{+-}(P^0,|\vec{k}'|)V^C(\vec{k}-\vec{k}')}{P^0-2E(\vec{k}')}. \tag{2.16}$$

A similar analysis leads to

$$\Gamma_5^{-+}(P^0,|\vec{k}|)=1+\int\frac{d^3k'}{(2\pi)^3}\left[\frac{m^2-2E(\vec{k})E(\vec{k}')}{E(\vec{k})E(\vec{k}')}\right]\times\frac{\Gamma_5^{-+}(P^0,|\vec{k}'|)V^C(\vec{k}-\vec{k}')}{P^0+2E(\vec{k}')}. \tag{2.17}$$

For example, Eq. (2.16) is obtained if we complete the integral in the lower complex k_0' plane and pick up *only* the pole where the quark is on its positive mass shell [8]. The other pole in the lower-half k_0' plane corresponds to the antiquark being on its negative mass shell. [It plays a role when we obtain Eq. (2.17).] Note that when $P^0-2E(\vec{k})=0$, $\Gamma^{+-}(P^0,|\vec{k}|)=0$. This aspect of the confinement model removes the unphysical $q\overline{q}$ cuts that would otherwise appear in the vacuum polarization integrals, $J(P^2)$. Using these results we find

$$J^{PP}(P^2)=-2n_cn_f\int\frac{d^3k}{(2\pi)^3}\left[\frac{\Gamma_5^{+-}(P^0,|\vec{k}|)}{P^0-2E(\vec{k})}-\frac{\Gamma_5^{-+}(P^0,|\vec{k}|)}{P^0+2E(\vec{k})}\right]. \tag{2.18}$$

Since the second term is small, except at low energy, and $\Gamma_5^{-+}(P^0,|\vec{k}|)$ is fairly close to unity, we will use the approximation

$$J^{PP}(P^2)=-2n_cn_f\int\frac{d^3k}{(2\pi)^3}\left[\frac{\Gamma_5^{+-}(P^0,|\vec{k}|)}{P^0-2E(\vec{k})}-\frac{1}{P^0+2E(\vec{k})}\right] \tag{2.19}$$

in the intermediate energy region. In the absence of confinement ($\kappa=0$) we put $\Gamma_5^{+-}(P^0,|\vec{k}|)=1$ in Eq. (2.19).

We also need to introduce a longitudinal axial-vector vertex, $\bar{\Gamma}_L^{\mu}$, in the calculation of $J_{\mu\nu}^{AA}(P)$. We write, for $\vec{P}=0$,

$$\Lambda^{(+)}(\vec{k})\Gamma_L^{\mu}(P,k)\Lambda^{(-)}(-\vec{k})=\frac{P^{\mu}}{\sqrt{P^2}}\Gamma_L^{+-}(P,k)\times\Lambda^{(+)}(\vec{k})\gamma_5\Lambda^{(-)}(-\vec{k}). \tag{2.20}$$

Now note that from Eq. (2.10)

$$P^2J_L^{AA}(P^2)=-P^{\mu}J_{\mu\nu}^{AA}(P)P^{\nu}, \tag{2.21}$$

so that, including $\bar{\Gamma}_L^{\mu}$ at one vertex, we have

$$P^2J_L^{AA}(P^2)=-n_cn_fi\int\frac{d^4k}{(2\pi)^4}\mathrm{Tr}[S(P/2+k)P^{\mu}\bar{\Gamma}_{\mu}(P,k)\times S(-P/2+k)\not{P}\gamma_5]. \tag{2.22}$$

Completing the integral in the lower k^0 plane and picking up the contribution of both poles of the propagators found there, we obtain

$$J_L^{AA}(P^2)=2n_cn_f\int\frac{d^3k}{(2\pi)^3}\frac{m}{E(\vec{k})}\left[\frac{\Gamma_L^{+-}(P^0,|\vec{k}|)}{P^0-2E(\vec{k})}-\frac{m/E(\vec{k})}{P^0+2E(\vec{k})}\right]. \tag{2.23}$$

[See Eq. (2.27).] Here we have neglected confinement in the second term of Eq. (2.23). In the absence of a confinement model ($\kappa=0$), $\Gamma_L^{+-}(P^0,|\vec{k}|)=m/E(\vec{k})$, so that

$$J_L^{AA}(P^2)=2n_cn_f\int\frac{d^3k}{(2\pi)^3}\left[\frac{m}{E(\vec{k})}\right]^2\frac{4E(\vec{k})}{(P^0)^2-[2E(\vec{k})]^2}, \tag{2.24}$$

for $P^0<2m$. Note that in the low-energy regime, $P^2\leq 0.10\,\mathrm{GeV}^2$, we will use Eq. (2.24) and for the intermediate-energy regime, we will use Eq. (2.23) when calculating polarization integrals. As noted above, an important feature of our confinement vertex functions is that they are zero when the quark and antiquark both go on their (positive) mass shells. Therefore, expressions such as $\Gamma_5^{+-}(P^0,|\vec{k}|)/[P^0-2E(\vec{k})]$ and $\Gamma_L^{+-}(P^0,|\vec{k}|)/[P^0-2E(\vec{k})]$ are finite. Thus, we need not include a term such as $i\epsilon$ in the denominators of these expressions.

An equation for the longitudinal axial-vector vertex is obtained by starting with

$$\bar{\Gamma}_L^{\mu}(P,k)=\frac{P^{\mu}\not{P}}{P^2}\gamma_5-i\int\frac{d^4k'}{(2\pi)^4}\gamma^{\rho}S(P/2+k')\bar{\Gamma}_L^{\mu}(P,k')\times S(-P/2+k')\gamma_{\rho}V^C(\vec{k}-\vec{k}'), \tag{2.25}$$

and using Eq. (2.20). Thus

$$\frac{P^{\mu}}{\sqrt{P^2}}\Lambda^{(+)}(\vec{k})\gamma_5\Lambda^{(-)}(-\vec{k})\Gamma_L^{+-}(P,k)=\frac{P^{\mu}}{P^2}\Lambda^{(+)}(\vec{k})\not{P}\gamma_5\Lambda^{(-)}(-\vec{k})+\frac{iP^{\mu}}{\sqrt{P^2}}\int\frac{d^4k'}{(2\pi)^4}\frac{\Lambda^{(+)}(\vec{k})\gamma^{\rho}\Lambda^{(+)}(\vec{k}')\gamma_5\Lambda^{(-)}(-\vec{k}')\gamma_{\rho}\Lambda^{(-)}(-\vec{k})}{\left[\frac{P^2}{2}+k^{0'}-E(\vec{k}')+i\epsilon\right]\left[-\frac{P^0}{2}+k^{0'}+E(\vec{k}')-i\epsilon\right]}\times\left[\frac{m}{E(k')}\right]^2V^C(\vec{k}-\vec{k}')\Gamma_L^{+-}(P,k'), \tag{2.26}$$

where, for simplicity we have neglected the coupling of Γ_L^{+-} to Γ_L^{-+}. If we multiply Eq. (2.26) by γ_5 and take the trace, we find

$$\Gamma_L^{+-}(P^0,|\vec{k}|)=\frac{m}{E(\vec{k})}+\int\frac{d^3k'}{(2\pi)^3}\left[\frac{2E(\vec{k}')E(\vec{k})-m^2}{E(\vec{k})E(\vec{k}')}\right]\times\frac{\Gamma_L^{+-}(P^0,|\vec{k}'|)}{P^0-2E(\vec{k}')}V^C(\vec{k}-\vec{k}'). \quad (2.27)$$

We can also show that

$$\Gamma_L^{-+}(P^0,|\vec{k}|)=-\frac{m}{E(\vec{k})}-\int\frac{d^3k'}{(2\pi)^3}\left[\frac{2E(\vec{k}')E(\vec{k})-m^2}{E(\vec{k})E(\vec{k}')}\right]\times\frac{\Gamma_L^{-+}(P^0,|\vec{k}'|)}{P^0+2E(\vec{k}')}V^C(\vec{k}-\vec{k}'). \quad (2.28)$$

[Thus, in the absence of confinement $\Gamma_L^{+-}(P^0,|\vec{k}|)=m/E(\vec{k})$, as note above. Therefore, we obtain Eq. (2.24) from Eq. (2.23), if $\kappa=0$.] Note that Eqs. (2.16) and (2.27) are rather similar, with the *homogeneous* equations being identical. Thus, $\Gamma_5^{+-}(P^0,|\vec{k}|)$ and $\Gamma_L^{+-}(P^0,|\vec{k}|)$ have singularities at the same values of P^0. These singularities correspond to bound states in the confining field considered in isolation. (If we consider only the confining interaction, these bound states appear as doublets.)

Proceeding in an analogous fashion as in our calculations of $J^{PP}(P^2)$ and $J^{AA}(P^2)$, we find

$$J^{PA}(P^2)=-2n_cn_f\int\frac{d^3k}{(2\pi)^3}\frac{m}{E(\vec{k})}\times\left[\frac{\Gamma_5^{+-}(P^0,|\vec{k}|)}{P^0-2E(\vec{k})}+\frac{1}{P^0+2E(\vec{k})}\right]. \quad (2.29)$$

For $\kappa=0$, we see that

$$J^{PA}(P^2)=-4P^0n_cn_f\int\frac{d^3k}{(2\pi)^3}\left[\frac{m}{E(\vec{k})}\right]\frac{1}{(P^0)^2-[2E(\vec{k})]^2}, \quad (2.30)$$

with $J^{PA}(0)=J^{AP}(0)=0$. We will use Eq. (2.30) in the low-energy domain and Eq. (2.29) in the intermediate-energy domain, where the second term in Eq. (2.29) is quite small.

As is well known, the integrals defining the vacuum polarization functions are divergent. Therefore, they are cut off by inserting a theta function $\theta(\Lambda_3-|\vec{k}|)$. We used $\Lambda_3=0.622\,\mathrm{GeV}$ in our earlier work and we continue to use that value here. (With $m=0.364\,\mathrm{GeV}$ and $\Lambda_3=0.622\,\mathrm{GeV}$, one obtains satisfactory values for the vacuum condensates $\langle\overline{u}u\rangle$ and $\langle\overline{d}d\rangle$, and for the pion decay constant f_π [1].) At a later point in our discussion, we will introduce a covariant version of our cutoff function.

III. RESONANCES AND MIXING ANGLES

The resonant states of the coupled pseudoscalar and longitudinal axial-vector fields may be found by studying the T matrix for $q\overline{q}$ scattering, including channel coupling terms. In the absence of such coupling $[J^{PA}(P^2)=0]$ the T matrix in the pion channel is

$$T_\pi(P^2)=i\gamma_5T^{PP}(P^2)i\gamma_5, \quad (3.1)$$

where

$$T_\pi^{PP}(P^2)=-\frac{G_S}{1-G_SJ^{PP}(P^2)}, \quad (3.2)$$

with $1-G_SJ^{PP}(m_\pi^2)=0$. If we include channel coupling we write

$$\hat{T}=i\gamma_5T^{PP}(P^2)i\gamma_5+i\gamma_5iT^{PA}(P^2)\frac{\not{P}}{\sqrt{P^2}}\gamma_5+\frac{\not{P}\gamma_5}{\sqrt{P^2}}iT^{AP}(P^2)i\gamma_5+\frac{\not{P}\gamma_5}{\sqrt{P^2}}T_L^{AA}(P^2)\frac{\not{P}\gamma_5}{\sqrt{P^2}}. \quad (3.3)$$

This form serves to define $T^{PP}(P^2)$, $T^{PA}(P^2)=-T^{AP}(P^2)$, and $T^{AA}(P^2)$. It is then useful to organize these quantities into a matrix

$$T(\mu,\nu)=\begin{pmatrix}T^{PP}(P^2) & iT^{PP}(P^2)P^\nu/\sqrt{P^2}\\ iT^{AP}(P^2)P^\mu/\sqrt{P^2} & T_L^{AA}(P^2)P^\mu P^\nu/P^2\end{pmatrix}. \quad (3.4)$$

In a similar fashion, we may define

$$J(\beta,\rho)=\begin{pmatrix}J^{PP}(P^2) & iJ^{PA}(P^2)P^\rho/\sqrt{P^2}\\ iJ^{AP}(P^2)P^\beta/\sqrt{P^2} & -J_L^{AA}(P^2)P^\beta P^\rho/P^2\end{pmatrix} \quad (3.5)$$

and also define the matrix

$$G(\mu,\nu)=\begin{pmatrix}G_S & 0\\ 0 & -G_Vg_L^{\mu\nu}\end{pmatrix}, \quad (3.6)$$

where $g_L^{\mu\nu}=P^\mu P^\nu/P^2$. Thus, we may write the equation

$$T(\mu,\nu)=-G(\mu,\nu)+G(\mu,\beta)J(\beta,\rho)T(\rho,\nu), \quad (3.7)$$

where the repeated Lorentz indices are summed.

The resulting equations may be usefully written in the following matrix form:

$$\begin{pmatrix}1-G_SJ^{PP}(P^2) & -iG_SJ^{PA}(P^2)\\ iG_VJ^{AP}(P^2) & 1-G_VJ_L^{AA}(P^2)\end{pmatrix}\begin{pmatrix}T^{PP}(P^2) & iT^{PA}(P^2)\\ iT^{AP}(P^2) & T_L^{AA}(P^2)\end{pmatrix}=-\begin{pmatrix}G_S & 0\\ 0 & -G_V\end{pmatrix}. \quad (3.8)$$

We can call the first matrix on the left-hand side of Eq. (3.8) $D(P^2)$, with

$$\det D(P^2)=[1-G_SJ^{PP}(P^2)][1-G_VJ_L^{AA}(P^2)]+G_SG_V[J^{PA}(P^2)]^2, \quad (3.9)$$

where we have used the fact that $J^{AP}(P^2) = -J^{PA}(P^2)$.

The solution of the matrix equation, Eq. (3.8), is

$$T^{PP}(P^2) = -\frac{G_S[1 - G_V J_L^{AA}(P^2)]}{\det D(P^2)}, \tag{3.10}$$

$$T^{PA}(P^2) = \frac{G_V G_S J^{PA}(P^2)}{\det D(P^2)}, \tag{3.11}$$

$$T^{AA}(P^2) = \frac{G_V[1 - G_S J^{PP}(P^2)]}{\det D(P^2)}, \tag{3.12}$$

with $T^{AP}(P^2) = -T^{PA}(P^2)$, Note that bound (or resonant) states correspond to the zeros of $\det D(P^2)$.

Now consider the T matrix of Eq. (3.3) in the frame where $\vec{P} = 0$. We may write

$$\hat{T} = (i\gamma_5, \gamma^0\gamma_5)\begin{pmatrix} T^{PP}(P^2) & iT^{PA}(P^2) \\ iT^{AP}(P^2) & T_L^{AA}(P^2) \end{pmatrix}\begin{pmatrix} i\gamma_5 \\ \gamma^0\gamma_5 \end{pmatrix}, \tag{3.13}$$

which may be written as $\Phi^T T(P^2)\Phi$. Now we use the matrices

$$M(\theta) = \begin{pmatrix} \cos\theta & i\sin\theta \\ i\sin\theta & \cos\theta \end{pmatrix} \tag{3.14}$$

and

$$M^{-1}(\theta) = \begin{pmatrix} \cos\theta & -i\sin\theta \\ -i\sin\theta & \cos\theta \end{pmatrix}, \tag{3.15}$$

to bring $T(P^2)$ of Eq. (3.13) to diagonal form:

$$M(\theta)T(P^2)M^{-1}(\theta) = \begin{pmatrix} T_1(P^2) & 0 \\ 0 & T_2(P^2) \end{pmatrix}. \tag{3.16}$$

We find a P^2-dependent mixing angle,

$$\tan 2\theta(P^2) = \frac{2T^{PA}(P^2)}{T^{PP}(P^2) - T^{AA}(P^2)}. \tag{3.17}$$

Values for $T_1(P^2)$, $T_2(P^2)$, $\det D(P^2)$, and $\theta(P^2)$ will be presented in Sec. IV for the low-energy region and in Sec. V for the intermediate-energy region.

IV. π-a_1 MIXING AT LOW ENERGY

As noted in the Introduction, it is best to neglect confinement at low energy in our model, where it represents only a small effect. In this work we neglect confinement for $P^2 \leq 0.1\,\mathrm{GeV}^2$. We show $J^{PP}(P^2)$, $J^{PA}(P^2)$, and $J^{AA}(P^2)$ in Figs. 3, 4, and 5, respectively. In Fig. 6 we show $\det D(P^2)$. We use $G_V = 12.50\,\mathrm{GeV}^{-2}$, a value that was used in our earlier work [4]. We find that the choice $G_S = 11.83\,\mathrm{GeV}^{-2}$ yields a pion mass of 138 MeV. (See Fig. 6.)

In Fig. 7, we show the value of $T_1(P^2)$. We do not show $T_2(P^2)$, since that function is, more or less, constant in the region $0 \leq P^2 \leq 0.1\,\mathrm{GeV}^2$. In Fig. 8 we show the mixing angle, $\theta(P^2)$, for the low-energy region. We find that $\theta(m_\pi^2) = -3.39°$, which represents a small admixture of the longitudinal axial-vector state. This admixture has a number of interesting physical consequences as described in Ref. [1].

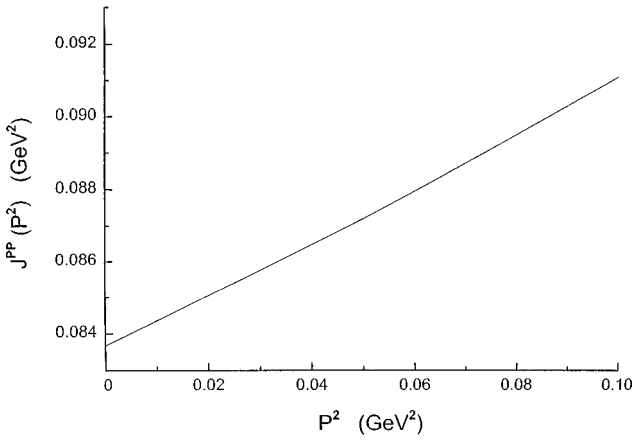

FIG. 3. The function $J^{PP}(P^2)$ is shown in the low-energy region. Here $m = 0.364\,\mathrm{GeV}$ and $\Lambda_3 = 0.622\,\mathrm{GeV}$.

The introduction of confinement tends to reduce the polarization integrals, $J(P^2)$, by about 10% at low energies. We can make the values of $\det D(P^2)$, $T_1(P^2)$, and $T_2(P^2)$ continuous as we go from below $P^2 = 0.1\,\mathrm{GeV}^2$ to above that value by increasing G_S from 11.83 GeV^{-2} to 12.80 GeV^{-2} when we introduce confinement. We use the latter value to obtain the results reported in Sec. V. While we are not too concerned with the dynamics in the low-energy region in this work, it may be of interest to consider a smooth turning on of the confining interaction. That may be accomplished by writing

$$\kappa(P^2) = \kappa(1 - e^{-\alpha P^2}). \tag{4.1}$$

We see that $\kappa(0) = 0$ and, if $\alpha = 7.67\,\mathrm{GeV}^2$, we have $\kappa(0.3\,\mathrm{GeV}^2) = 0.9\kappa$. The use of this scheme yields the values of $J^{PP}(P^2)$, $J^{PA}(P^2)$, and $J^{AA}(P^2)$ shown in Figs. 9, 10, and 11, respectively, for the region $0 \leq P^2 \leq 0.3\,\mathrm{GeV}^2$. Here, we use $\kappa = 0.0575\,\mathrm{GeV}^2$, the value used in our earlier work on light-meson spectroscopy [4,5]. (We also use $m = 0.364\,\mathrm{GeV}$ and $\Lambda_3 = 0.622\,\mathrm{GeV}$, which are also values used in our earlier work [4,5].)

The vertical lines in Figs. 9–11 show the positions of the bound states in the confining field. They represent the singularities of the vertex functions Γ_5^{+-} and Γ_L^{+-}. Recall that Γ_5^{+-} and Γ_L^{+-} satisfy inhomogeneous equations and these functions are singular when the homogeneous equations have solutions. [The homogeneous equation is an equation for the vertex function of the bound states in the field set up by the potential $V^C(\vec{k} - \vec{k}')$.]

V. π-a_1 MIXING AT INTERMEDIATE ENERGY

In this section we make use of the values of $J^{PP}(P^2)$, $J^{PA}(P^2)$, and $J^{AA}(P^2)$ shown in Figs. 9–11. With $G_S = 12.80\,\mathrm{GeV}^{-2}$ and $G_V = 12.50\,\mathrm{GeV}^{-2}$, we find the values of $\det D(P^2)$ shown in Fig. 12. There are zeros of $\det D(P^2)$ at $P^0 = 1.18$, 1.36, 1.47, 1.63, and 1.68 GeV, in addition to the zero at $P^0 = 0.138\,\mathrm{GeV}$ shown in Fig. 6. We recall that these are all $J^P = 0^-$ states, while the data tables only list the $\pi(1300)$ in the energy region considered in this section. Our states appear in either $T_1(P^2)$, shown in Fig. 13, or $T_2(P^2)$,

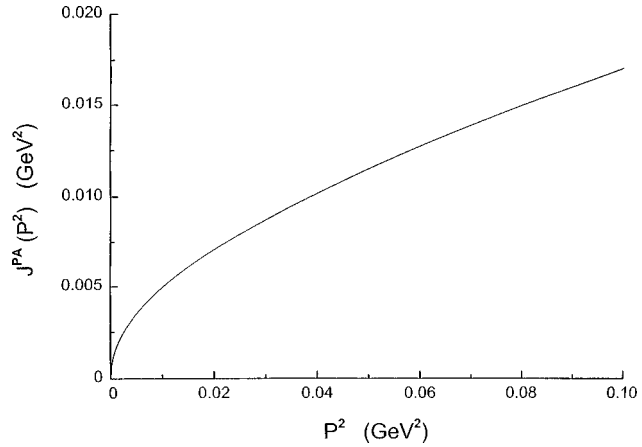

FIG. 4. The function $J^{PA}(P^2)$ is shown in the low-energy region.

shown in Fig. 14. Specifically, in $T_1(P^2)$ we find resonances at $P^0=0.138$, 1.18, 1.63, and 1.68 GeV, while $T_2(P^2)$ has such states at $P^0=1.36$ and 1.47 GeV. Table I gives the value of the mixing angle $\theta(P^2)$ for the pion and for the five resonances listed above. (See Fig. 15.) Again, with reference to Table I, we see that the resonance at 1.63 GeV is in the channel $T_1(P^2)$. Therefore, we can state that the resonance is ''pionlike,'' since the mixing angle is very small.

In order to calculate the decay amplitudes of our states, we will calculate the loop integrals shown in Fig. 16. If we calculate the quark loop of Fig. 16(a), we find unphysical singularities when $q\overline{q}$ pairs go on mass shell, as indicated in Figs. 16(b) and 16(c). One way to deal with this problem is to include vertex functions of a confining interaction, as indicated in Fig. 16(d). As we will see, these vertex functions are equal to zero, when both the quark and antiquark go on their (positive) mass shells. This feature serves to eliminate the singularities indicated in Figs. 16(b) and 16(c).

In the next section we will show how the vertex functions of the confining interaction are calculated, with the aim of the making covariant calculations of the loop diagrams of Fig. 16.

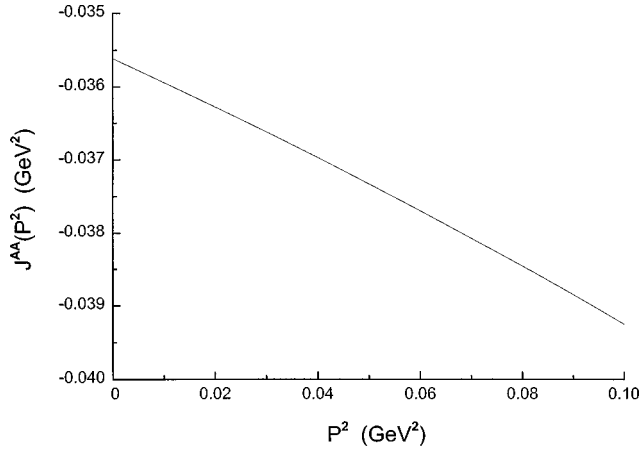

FIG. 5. The function $J^{AA}(P^2)$ is shown in the low-energy region.

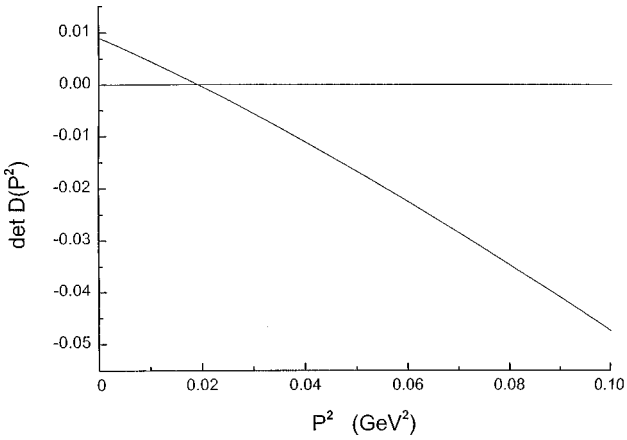

FIG. 6. The function $\det D(P^2)$ is shown in the low-energy region. Note that $\det D(m_\pi^2)=0$. Here $G_S=11.83\,\mathrm{GeV}^{-2}$ and $G_V=12.50\,\mathrm{GeV}^{-2}$.

VI. PSEUDOSCALAR VERTEX FUNCTION FOR THE CONFINING INTERACTION

Vertex functions may be constructed for the calculation of the properties of mesons of various angular momenta. The (inhomogeneous) equation defining the vertex function is depicted in Fig. 2(a). (For example, for the pseudoscalar vertex function, the driving term would be $\gamma_5\tau^a$, where τ^a is an isospin matrix.) In Fig. 2(a) V^C represents the confining interaction, which, in our model, may be expressed in terms of the square of the difference of two four-vectors, $V^C[(k_c-k_c')^2]$, where

$$k_c^\mu = k^\mu - \frac{(k\cdot P)P^\mu}{P^2} \tag{6.1}$$

and

$$k_c'^\mu = k'^\mu - \frac{(k'\cdot P)P^\mu}{P^2}. \tag{6.2}$$

Note that the invariant $-k_c^2$ may be identified as the square of the relative three-momentum, $\vec{k}^2$, of the quark and antiquark in the meson rest frame where $\vec{P}=0$. (Later in this

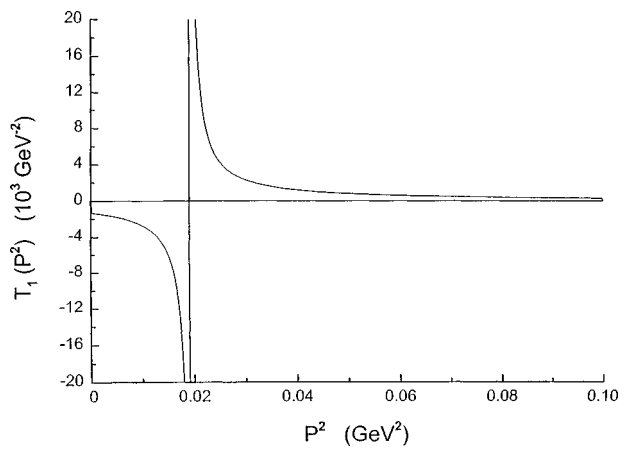

FIG. 7. The function $T_1(P^2)$ is shown in the low-energy region. The singularity at $P^2=m_\pi^2$ is indicated by the vertical line.

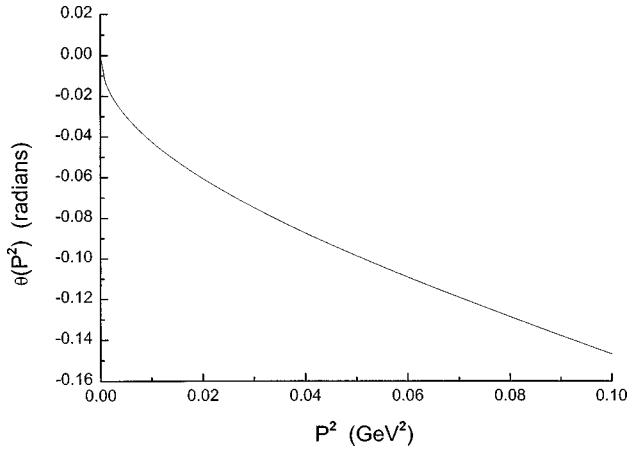

FIG. 8. The mixing angle, $\theta(P^2)$, is shown in the low-energy region. Note that $\theta(m_\pi^2) = -3.39°$.

work we will introduce four-vectors $\hat{k}^\mu$ and $\hat{k}'^\mu$ that are defined in the same fashion as k_c^μ and $k_c'^\mu$. We use the notation k_c^μ and $k_c'^\mu$ when we wish to stress the role of these vectors in providing the value of $\vec{k}^2$ defined above.) In the meson's rest frame, we have $k_c^\mu = (0,\vec{k})$ and $k_c'^\mu = (0,\vec{k}')$. When $\vec{P} = 0$, we obtain the Fourier transform of $V^C(\vec{r})$ given in Eq. (2.3), which is a form we have used in earlier work. (Equation (2.3) provides the Fourier transform of the potential $V^C(\vec{r}) = \kappa r \exp[-\mu r]$. While this potential is not absolutely confining, μ is chosen small enough so that the potential is effectively linear over the region of $|\vec{r}|$ relevant to the problem considered. Effects of barrier penetration are found to be negligible.) In this work we use Lorentz-vector confinement, so that we need to include a Dirac matrix, γ^ρ, at the points where the potential is coupled to a quark or an antiquark.

It is convenient to work in the frame where $\vec{P} = 0$ and study the equation shown in Fig. 2. Let us consider the pseudoscalar vertex and the scalar functions $\Gamma_5^{+-}(P,k)$ and $\Gamma_5^{-+}(P,k)$, introduced earlier. When creating a covariant model, it is useful to write $\Gamma_5^{+-}(\sqrt{P^2},\sqrt{-k_c^2})$, etc. For the covariant model, we define

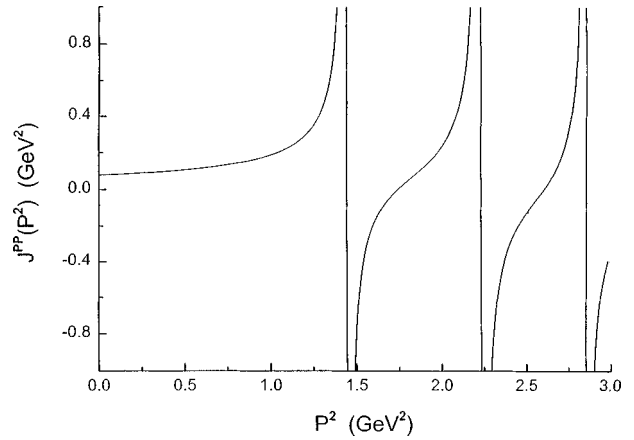

FIG. 9. The function $J^{PP}(P^2)$ is shown for $0 \leqslant P^2 \leqslant 3.0\ \mathrm{GeV}^2$. Here $\kappa = 0.0575\ \mathrm{GeV}^2$ and $m = 0.364\ \mathrm{GeV}$. A cutoff $\theta(\Lambda_3 - |\vec{k}|)$ is used, with $\Lambda_3 = 0.622\ \mathrm{GeV}$.

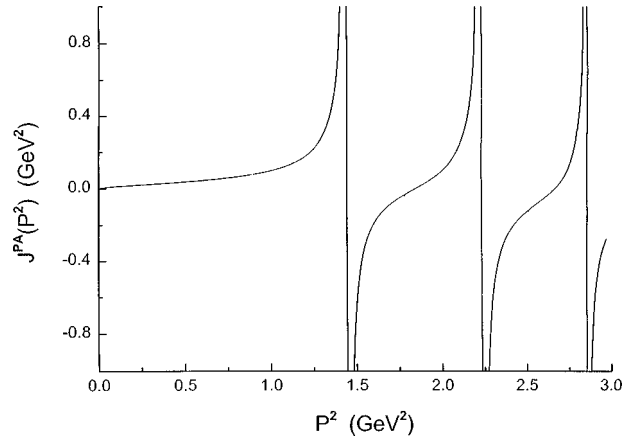

FIG. 10. The function $J^{PA}(P^2)$ is shown for $0 \leqslant P^2 \leqslant 3.0\ \mathrm{GeV}^2$.

$$\overline{\Gamma}_5(P,k) = \gamma_5[b_0(\sqrt{P^2},\sqrt{-k_c^2}) + \not{P}\, b_1(\sqrt{P^2},\sqrt{-k_c^2})]. \tag{6.3}$$

It is not difficult to see that, when $\vec{P} = 0$,

$$\Gamma_5^{+-}(\sqrt{P^2},\sqrt{-k_c^2}) = b_0(\sqrt{P^2},\sqrt{-k_c^2}) - \frac{mP^0}{E(\vec{k})} b_1(\sqrt{P^2},\sqrt{-k_c^2}) \tag{6.4}$$

and

$$\Gamma_5^{-+}(\sqrt{P^2},\sqrt{-k_c^2}) = b_0(\sqrt{P^2},\sqrt{-k_c^2}) + \frac{mP^0}{E(\vec{k})} b_1(\sqrt{P^2},\sqrt{-k_c^2}). \tag{6.5}$$

We can solve these equations for the Lorentz scalars, b_0 and b_1, once Γ^{+-} and Γ^{-+} are calculated in the frame where $\vec{P} = 0$. This procedure yields the *covariant* form for $\overline{\Gamma}_5(P,k)$ given in Eq. (6.3), which can be used for finite values of $\vec{P}$. Note that, for $\vec{P} = 0$,

$$b_0(\sqrt{P^2},k_{\mathrm{on}}) - 2m b_1(\sqrt{P^2},k_{\mathrm{on}}) = 0, \tag{6.6}$$

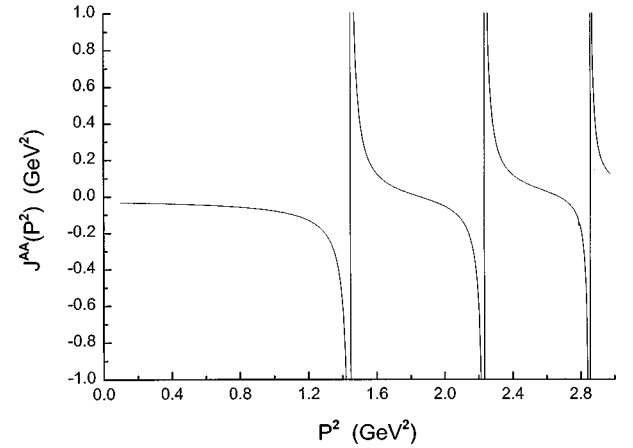

FIG. 11. The function $J^{AA}(P^2)$ is shown for $0.10 \leqslant P^2 \leqslant 3.0\ \mathrm{GeV}^2$.

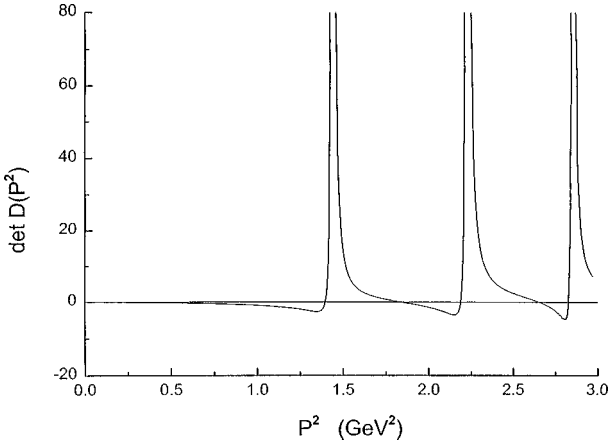

FIG. 12. The function $\det D(P^2)$ is shown. Here $G_S = 12.80\ \mathrm{GeV}^{-2}$, $G_V = 12.50\ \mathrm{GeV}^2$, and $\kappa = 0.0575\ \mathrm{GeV}^2$.

when $k_{\mathrm{on}}^2 = (P^0)^2/4 - m^2$. At that point, $P^0 = 2E(\vec{k})$. [See Eq. (6.4).] It is the zero value given in Eq. (6.6) that serves to remove unphysical singularities from the various amplitudes we calculate. Equations for $\Gamma_5^{+-}(P^0,|\vec{k}|)$ and $\Gamma_5^{-+}(P^0,|\vec{k}|)$ were given previously. [See Eqs. (2.16) and (2.17).] Note that $\Gamma^{+-}(P^0,|\vec{k}|)/[P^0 - 2E(\vec{k})]$ is finite, so that one does not need to write an $i\epsilon$ in the denominator. [It is convenient to solve Eqs. (2.16) and (2.17) for $\Psi(P^0,|\vec{k}|) = \Gamma^{+-}(P^0,|\vec{k}|)/[P^0 - 2E(\vec{k})]$ and then obtain $\Gamma^{+-}(P^0,|\vec{k}|)$ from $\Psi(P^0,|\vec{k}|)$ by multiplying by $P^0 - 2E(\vec{k})$.]

The coupling between Γ_5^{+-} and Γ_5^{-+} gives rise to ''Z graphs,'' which we neglect. While such coupling may be taken into account for scalar, vector, and axial-vector vertices, in the case of the pseudoscalar vertex the coupling is so large as to preclude the solution of the *coupled* equations for Γ_5^{+-} and Γ_5^{-+}. Therefore, our analysis is based upon the use of Eqs. (2.16) and (2.17).

We now introduce functions d_0 and d_1:

$$\bar{\Gamma}_L(P,k) = \frac{\not{P}}{\sqrt{P^2}}\gamma_5[d_0(\sqrt{P^2},\sqrt{-k_c^2}) + \not{P}\, d_1(\sqrt{P^2},\sqrt{-k_c^2})]. \tag{6.7}$$

In the rest frame ($\vec{P} = 0$), the last equation reads

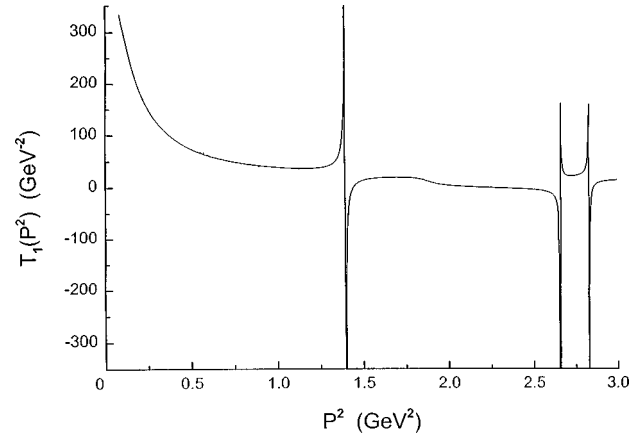

FIG. 13. The function $T_1(P^2)$ is shown. The vertical lines indicate the positions of the singularities of this function.

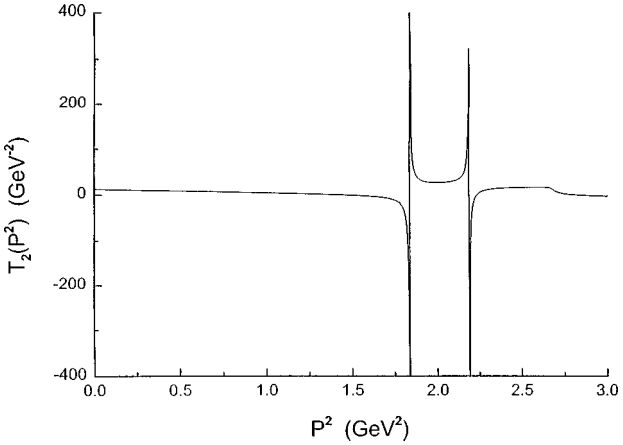

FIG. 14. The function $T_2(P^2)$ is shown. (See caption to Fig. 13.)

$$\bar{\Gamma}_L(P^0,|\vec{k}|) = \gamma_0\gamma_5[d_0(P^0,|\vec{k}|) + \gamma_0 P^0 d_1(P^0,|\vec{k}|)]. \tag{6.8}$$

Therefore

$$\bar{\Gamma}_L^{+-}(P^0,|\vec{k}|) = \frac{m}{E(k)}d_0(P^0,|\vec{k}|) - P^0 d_1(P^0,|\vec{k}|) \tag{6.9}$$

and

$$\bar{\Gamma}_L^{-+}(P^0,|\vec{k}|) = -\frac{m}{E(k)}d_0(P^0,|\vec{k}|) - P^0 d_1(P^0,|\vec{k}|). \tag{6.10}$$

Thus,

$$d_0(P^0,|\vec{k}|) = \frac{E(k)}{2m}[\Gamma_L^{+-}(P^0,|\vec{k}|) - \Gamma_L^{-+}(P^0,|\vec{k}|)], \tag{6.11}$$

$$d_1(P^0,|\vec{k}|) = -\frac{1}{2P^0}[\Gamma_L^{+-}(P^0,|\vec{k}|) + \Gamma_L^{-+}(P^0,|\vec{k}|)]. \tag{6.12}$$

With these definitions, we can show how the vertex functions that appear in the T matrix are modified by the confining interaction. We recall that

TABLE I. Values of the mixing angle for various bound or resonant states. For a resonance in the T_2 channel, we may use the formalism for a resonance in the T_1 channel, if we add 90° to the angle given in the table. Thus the 1.36 GeV state and the 1.47 GeV state would be assigned the values $\theta = 2.2°$ and $\theta = 122°$, respectively.

Energy (GeV)	Channel	θ (radians)	θ (degrees)
0.138	T_1	−0.059	−3.39°
1.18	T_1	2.20	126°
1.36	T_2	−1.52	−87.8°
1.47	T_2	0.55	31.8°
1.63	T_1	0.047	2.68°
1.68	T_1	2.06	118°

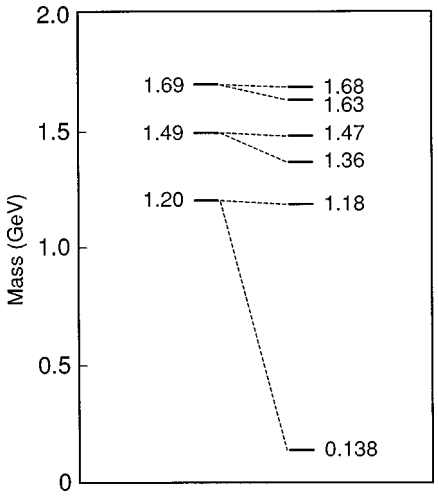

FIG. 15. The energies of the doublets in the confining field are shown in the left-hand side of the figure. The energies of the states obtained when the short-range NJL interaction is added are shown on the right-hand side of the figure.

$$M\begin{pmatrix} i\gamma_5 \\ \gamma^0\gamma_5 \end{pmatrix}=\begin{pmatrix} i\cos\theta\gamma_5+i\sin\theta\gamma^0\gamma_5 \\ -\sin\theta\gamma_5+\cos\theta\gamma^0\gamma_5 \end{pmatrix}. \tag{6.13}$$

The upper line provides the vertex for resonances in T_1 and the lower line provides the vertex for resonances in T_2.

If we sum an infinite ''ladder'' of confining interactions the right-hand side of Eq. (6.13) is replaced by

$$\Phi_c=\begin{pmatrix} i\cos\theta\gamma_5(b_0+\gamma^0P^0b_1)+i\sin\theta\gamma^0\gamma_5(d_0+\gamma^0P^0d_1) \\ -\sin\theta\gamma_5(b_0+\gamma^0P^0b_1)+\cos\theta\gamma^0\gamma_5(d_0+\gamma^0P^0d_1) \end{pmatrix} \tag{6.14}$$

with a straightforward generalization to the case with $\vec{P}\neq 0$,

$$\Phi_c=\begin{pmatrix} i\cos\theta\gamma_5(b_0+\not{P}b_1)+i\sin\theta\dfrac{\not{P}}{\sqrt{P^2}}\gamma_5(d_0+\not{P}d_1) \\ -\sin\theta\gamma_5(b_0+\not{P}b_1)+\cos\theta\dfrac{\not{P}}{\sqrt{P^2}}\gamma_5(d_0+\not{P}d_1) \end{pmatrix}. \tag{6.15}$$

VII. SCALAR VERTEX FOR THE CONFINING INTERACTION

The scalar vertex for a confining interaction was discussed in the first paper listed in Ref. [2]. We may write, in the case that our model has zero energy transfer in the frame with $\vec{P}=0$,

$$\overline{\Gamma}_S(P,k)=c_0(P,k)+\not{\hat{k}}\,c_1(P,k), \tag{7.1}$$

with $\hat{k}^\mu=k^\mu-(k\cdot P)P^\mu/P^2$. We define

$$\Lambda^{(+)}(\vec{k})\overline{\Gamma}_S(P,k)\Lambda^{(-)}(-\vec{k})=\Gamma_S^{+-}(P,k)\Lambda^{(+)}(\vec{k})\Lambda^{(-)}(-\vec{k}) \tag{7.2}$$

and

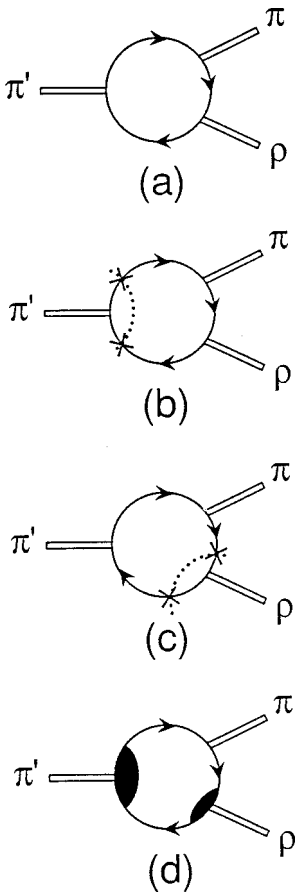

FIG. 16. (a) The decay of a π' to a π and a ρ meson at one-loop order is shown. (b) Quarks or antiquarks on their positive mass shell are denoted by crosses. In this case the decay of the π' to a $q\bar{q}$ pair gives rise to a singularity of the amplitude. The dotted line indicates the origin the singularity. (c) Similar caption to (b), except that ρ decay is responsible for singularities of the amplitude. (d) The amplitude of (a) is modified by including confinement vertex functions for the π' and the ρ. (See Fig. 2.) Confinement is only a small effect in the $\pi(138)$ vertex and is neglected in this work.

$$\Lambda^{(-)}(-\vec{k})\overline{\Gamma}_S(P,k)\Lambda^{(+)}(\vec{k})=\Gamma_S^{-+}(P,k)\Lambda^{(-)}(-\vec{k})\Lambda^{(+)}(\vec{k}). \tag{7.3}$$

The relations between Γ_S^{+-} and Γ_S^{-+} and c_0 and c_1 are

$$\Gamma_S^{+-}(P,k)=c_0(P,k)+mc_1(P,k), \tag{7.4}$$

and

$$\Gamma_S^{++}(P,k)=c_0(P,k)-\frac{\vec{k}^2}{m}c_1(P,k). \tag{7.5}$$

The formalism is made covariant by using Eq. (7.1) and the procedure described in Sec. VI.

Equations for Γ_S^{+-} and Γ_S^{-+} were given in the first paper of Ref. [2]. We repeat those equations here, taking the opportunity to correct two misprinted signs. With $k=|\vec{k}|$ and $k'=|\vec{k}'|$, we have

$$\Gamma_S^{+-}(P^0,|\vec{k}|)=1-4\pi\int\frac{k'^2dk'}{(2\pi)^3}\left[\frac{-8k'^2}{E(\vec{k}')}\right]\times\frac{V_0^C(k,k')+(m^2/2kk')V_1^C(k,k')}{(P^0)^2-[2E(\vec{k}')]^2}\times\Gamma_S^{+-}(P^0,k') \tag{7.6}$$

and

$$\Gamma_S^{++}(P^0,|\vec{k}|)=1-4\pi\int\frac{k'^2dk'}{(2\pi)^3}\left[\frac{-8k'^2}{E(\vec{k}')}\right]\times\frac{V_0^C(k,k')-(k/2k')V_1^C(k,k')}{(P^0)^2-[2E(\vec{k}')]^2}\Gamma_S^{+-}(P^0,k'). \tag{7.7}$$

In these equations

$$V_l^C(k,k')=\frac{1}{2}\int_{-1}^{1}dxP_l(x)V^C(\vec{k}-\vec{k}'). \tag{7.8}$$

Coupled equations for $c_0(P,k)$ and $c_1(P,k)$ are

$$c_0(P,k)=1-4\pi\int\frac{k'^2dk'}{(2\pi)^3}\left[\frac{-8k'^2}{E(\vec{k}')}\right]\times\frac{V_0^C(k,k')[c_0(P,k')+mc_1(P,k')]}{(P^0)^2-[2E(\vec{k}')]^2} \tag{7.9}$$

and

$$c_1(P,k)=4\pi\int\frac{k'^2dk'}{(2\pi)^3}\left[\frac{4mk'/k}{E(k')}\right]\times\frac{V_1^C(k,k')[c_0(P,k')+mc_1(P,k')]}{(P^0)^2-[2E(\vec{k}')]^2}, \tag{7.10}$$

where we have again corrected two misprinted signs that appear in the first paper of Ref. [2].

VIII. VECTOR VERTEX FUNCTION FOR THE CONFINING INTERACTION

In this section we introduce a vector vertex function $\Gamma^\mu(P,k)$ that sums a ladder of confining interactions. We express this function in terms of four Lorentz scalars and again use the four-vector

$$\hat{k}^\mu(P)=k^\mu-\frac{(k\cdot P)P^\mu}{P^2}. \tag{8.1}$$

[Recall that, in the frame where $\vec{P}=0$, $k^\mu=(0,\vec{k})$.] We also introduce the Dirac matrix

$$\hat{\gamma}^\mu=\gamma^\mu-\frac{\not{P}P^\mu}{P^2}, \tag{8.2}$$

with the property $\hat{\gamma}\cdot P=0$. In terms of that quantity, we define

$$\gamma_{\perp,k}^\mu=\hat{\gamma}^\mu-\frac{\hat{\not{k}}\hat{k}^\mu}{\hat{k}^2}, \tag{8.3}$$

such that $\hat{k}\cdot\gamma_{\perp,k}=0$. In Eq. (8.3) we have written $\hat{k}^\mu$ for $\hat{k}^\mu(P)$ for simplicity. With that simplified notation, we now define

$$\Gamma_V^\mu(P,k)=\frac{\hat{k}^\mu}{|\hat{k}^2|^{1/2}}\left[a_0(P,k)+\frac{\hat{\not{k}}}{|\hat{k}^2|^{1/2}}a_1(P,k)\right]+\gamma_{\perp,k}^\mu a_2(P,k)+i\epsilon^{\mu\nu\rho\sigma}\frac{\gamma_5\gamma_\nu P_\rho\hat{k}_\sigma a_3(P,k)}{|P^2|^{1/2}|\hat{k}^2|^{1/2}}. \tag{8.4}$$

In the frame where $\vec{P}=0$, we have

$$\vec{\Gamma}(P^0,|\vec{k}|)=\hat{\mathbf{k}}[a_0-\boldsymbol{\gamma}\cdot\hat{\mathbf{k}}a_1]+\boldsymbol{\gamma}_{\perp,k}a_2+i\gamma_5(\boldsymbol{\gamma}\times\hat{\mathbf{k}})a_3. \tag{8.5}$$

[In this case we can write $a_0(P^0,|\vec{k}|)$, etc.] In Eq. (8.5), $\hat{\mathbf{k}}$ is a unit vector along the direction of $\vec{k}$.

It is also useful to introduce eight scalar functions:

$$\Lambda^{(+)}(\hat{k})\vec{\Gamma}\Lambda^{(-)}(-\vec{k})=\Gamma_1^{+-}(P^0,|\vec{k}|)\hat{\mathbf{k}}\Lambda^{(+)}(\vec{k})\Lambda^{(-)}(-\vec{k})+\Gamma_2^{+-}(P^0,|\vec{k}|)\Lambda^{(+)}(\vec{k})\times\boldsymbol{\gamma}_{\perp,k}\Lambda^{(-)}(-\vec{k}), \tag{8.6}$$

$$\Lambda^{(-)}(-\vec{k})\vec{\Gamma}\Lambda^{(+)}(\vec{k})=\Gamma_1^{-+}(P^0,|\vec{k}|)\hat{\mathbf{k}}\Lambda^{(-)}(-\vec{k})\Lambda^{(+)}(\vec{k})+\Gamma_2^{-+}(P^0,|\vec{k}|)\Lambda^{(-)}(-\vec{k})\times\boldsymbol{\gamma}_{\perp,k}\Lambda^{(+)}(\vec{k}), \tag{8.7}$$

$$\Lambda^{(+)}(\vec{k})\vec{\Gamma}\Lambda^{(+)}(\vec{k})=\Gamma_1^{++}(P^0,|\vec{k}|)\hat{\mathbf{k}}\Lambda^{(+)}(\vec{k})\Lambda^{(+)}(\vec{k})+\Gamma_2^{++}(P^0,|\vec{k}|)\Lambda^{(+)}(\vec{k})\boldsymbol{\gamma}_{\perp,k}\Lambda^{(+)}(\vec{k}), \tag{8.8}$$

and

$$\Lambda^{(-)}(-\vec{k})\vec{\Gamma}\Lambda^{(-)}(-\vec{k})=\Gamma_1^{--}(P^0,|\vec{k}|)\hat{\mathbf{k}}\Lambda^{(-)}(-\vec{k})\times\Lambda^{(-)}(-\vec{k})+\Gamma_2^{--}(P^0,|\vec{k}|)\times\Lambda^{(-)}(\vec{k})\boldsymbol{\gamma}_{\perp,k}\Lambda^{(-)}(-\vec{k}). \tag{8.9}$$

Upon using Eq. (8.5), we find with $k=|\vec{k}|$,

$$\Gamma_1^{+-}=a_0+\frac{m}{k}a_1, \tag{8.10}$$

$$\Gamma_2^{+-}=a_2-\frac{k}{E(k)}a_3, \tag{8.11}$$

$$\Gamma_1^{-+}=\Gamma_1^{+-}, \tag{8.12}$$

$$\Gamma_2^{-+}=a_2+\frac{k}{E(k)}a_3, \tag{8.13}$$

$$\Gamma_1^{++}=a_0-\frac{k}{m}a_1, \tag{8.14}$$

$$\Gamma_2^{++}=a_3, \tag{8.15}$$

$$\Gamma_1^{--}=a_0+\frac{k}{m}a_1, \tag{8.16}$$

and

$$\Gamma_2^{--}=a_3. \tag{8.17}$$

In addition, it is useful to define a series of functions that go to 1 for large $|\vec{k}|$. These are $\gamma_1^{+-}=(-k/m)\Gamma_1^{+-}$, $\gamma_2^{+-}=\Gamma_2^{+-}$, $\gamma_1^{-+}=(-k/m)\Gamma_1^{-+}$, $\gamma_2^{-+}=\Gamma_2^{-+}$, $\gamma_1^{++}=(m/k)\Gamma_1^{++}$. We also define $\gamma_2^{++}=\Gamma_2^{++}$, $\gamma_1^{--}=(m/k)\Gamma_1^{--}$, and $\gamma_2^{--}=\Gamma_2^{--}$. The equations that are solved to obtain the various γ_i are presented in the Appendix. Once the γ_i are calculated, we obtain $a_0(P^0,|\vec{k}|)$, $a_1(P^0,|\vec{k}|)$, etc. The model is then made covariant by defining

$$a_i(\sqrt{P^2},\sqrt{-k_c^2})=a_i(P^0,|\vec{k}|), \tag{8.18}$$

for $i=0,1,2,3$. Thus, for finite $\vec{P}$, we may calculate $[-k_c^2]^{1/2}$ and use Eq. (8.18) to obtain the numerical value of the $a_i(\sqrt{P^2},\sqrt{-k_c^2})$. In the next section we show how this procedure leads to covariant calculations of a quark-loop diagrams describing meson decay which would have unphysical singularities in the absence of a confinement model. [We have also shown that this model provides a covariant result for vacuum polarization diagrams, if we replace the cutoff function $\theta(\Lambda_3^2-\vec{k}^2)$ by $\theta(\Lambda_3^2+k_c^2(P))$, with $k_c^\mu=k^\mu-(k\cdot P)P^\mu/P^2$.]

IX. COVARIANT CALCULATION OF THE AMPLITUDE FOR THE DECAY $\pi'\to\pi+\rho$

With reference to Fig. 16, we assign the four-momentum P to the π' and P' to the ρ. Thus the momentum of the final pion is $P-P'$. (If the π' is at rest, $\vec{P}=0$, and, if the ρ is at rest, $\vec{P}'=0$.) With i,j,k denoting the isospin indices, we define the amplitude

$$M_{ijk}^\mu(P,P')=n_c n_f i\epsilon^{ijk}\left(P^\mu-\frac{(P\cdot P')P'^\mu}{P'^2}\right)\times M(P^2,P'^2,P\cdot P'). \tag{9.1}$$

For simplicity, we do not include a confinement model for the final-state pion. There is no singularity to be removed at the pion vertex and confinement is only a small effect in this case. Thus, with $\beta=P^2-(P\cdot P')^2/P'^2$, we have

$$M(P^2,P'^2,P\cdot P')=\frac{i}{\beta}\int\frac{d^4k}{(2\pi)^4}\mathrm{Tr}\{[\Gamma_V(P',k)\cdot P]S(k+P')\gamma_5 S(k+P)\overline{\Gamma}_5(P,k)S(k)\} \tag{9.2}$$

$$=\frac{i}{\beta}\int\frac{d^4k}{(2\pi)^4}\frac{\mathrm{Tr}\{[\Gamma_V(P',k)\cdot P]T\}}{(k^2-m^2)((k+p)^2-m^2)((k+P')^2-m^2)}, \tag{9.3}$$

with

$$T=[(m+\not k+\not P')(m-(\not k+\not P))(b_0+\not P b_1)(m+\not k)]. \tag{9.4}$$

There is another diagram, with the ρ emitted first, that yields

$$M'(P^2,P'^2,P\cdot P')=-\frac{i}{\beta}\int\frac{d^4k}{(2\pi)^4}\frac{\mathrm{Tr}\{[\Gamma_V(P',-k)\cdot P]T'\}}{(k^2-m^2)((k+P)^2-m^2)((k+P')^2-m^2)}. \tag{9.5}$$

We found it convenient to send k^μ into $-k^\mu$ in the evaluation of this term. [The minus sign in Eq. (9.5) arises from the isospin trace.] In Eq. (9.5),

$$T'=[(m-\not k)(b_0-\not P b_1)(m+\not k+\not P)(m-(\not k+\not P'))]. \tag{9.6}$$

We remark that, if the final π and ρ are on mass shell, M is only a function of P^2 and, if the π' is also on mass shell, M is a constant. In evaluating the integrals in Eqs. (9.3) and (9.5) we include a cutoff function, $\theta(\Lambda_3^2+k_c^2(P))\theta(\Lambda_3^2+k_c^2(P'))$ which we do not exhibit for simplicity of notation. [Note that calculations may be made for the wave functions of Eqs. (6.14) or (6.15) by using effective values of b_0 and b_1 in Eq. (6.3).]

Combining M and M', a lengthy calculation of $M_T=M+M'$ yields

$$M_T(P^2,P'^2,P\cdot P')=\frac{i}{\beta}\int\frac{d^4k}{(2\pi)^4}\frac{\Sigma_{i=0}^{3}a_i(k_c')z_i(P,P',k)}{D(k)D(k+P)D(k+P')}, \tag{9.7}$$

with $D(k)=(k^2-m^2)$, etc. Here we have used a simplified notation for the a_i of Eq. (9.4), with

$$k_c'^{\mu}=k^{\mu}-\frac{(k\cdot P')P'^{\mu}}{m_\rho^2} \tag{9.8}$$

defined at the ρ vertex. We also use the notation

$$\hat{k}^{\mu}(P')=k^{\mu}-\frac{(k\cdot P')P'^{\mu}}{P'^2}, \tag{9.9}$$

and

$$\hat{k}^{\mu}(P)=k^{\mu}-\frac{(k\cdot P)P^{\mu}}{P^2}. \tag{9.10}$$

[Equation (9.10) was first introduced as Eq. (4.1).] In terms of these quantities we have

$$z_0(k,P,P')=\frac{\hat{k}(P')\cdot P}{|\hat{k}^2(P')|^{1/2}}\mathrm{Tr}(T+T') \tag{9.11}$$

with

$$\begin{aligned}\mathrm{Tr}(T+T')&=8\{mb_0[m^2-k^2-2k\cdot P-P\cdot P']+b_1[(k\cdot P)\\&\times[m^2-(k+P')\cdot(k+P)]+P\cdot(P-P')\\&+(k+P')\cdot P(k+P)\cdot k-(k+P')\cdot k(k+P)\cdot P]\}.\end{aligned} \tag{9.12}$$

Also,

$$z_1(k,P,P')=\frac{\hat{k}(P')\cdot P}{|\hat{k}^2(P')|^{1/2}}(\hat{k}^2(P')z_k+\hat{k}(P')\cdot Pz_p), \tag{9.13}$$

with

$$\begin{aligned}z_k=8\{&b_0[m^2-(k+P')\cdot(k+P)+k\cdot(P'-P)]\\&+2mb_1P\cdot(P'-P)\}\end{aligned} \tag{9.14}$$

and

$$z_p=8\{b_0[(k+P')\cdot k-m^2]+mb_1[m^2-(k^2+2k\cdot P')]\}. \tag{9.15}$$

In addition,

$$z_2(k,P,P')=\left[P^2-\frac{(P\cdot P')}{P'^2}-\frac{(\hat{k}(P')\cdot P)^2}{\hat{k}^2(P')}\right]z_p \tag{9.16}$$

and

$$\begin{aligned}z_3(k,P,P')=8\{&[P^2P'^2-(P\cdot P')^2]\hat{k}^2(P)\\&-P^2(\hat{k}(P)\cdot P')^2\}\frac{2mb_1-b_0}{[P^2]^{1/2}|\hat{k}^2(P')|^{1/2}}.\end{aligned} \tag{9.17}$$

As a next step, we complete the k^0 integral in the complex k^0 plane to find

$$\begin{aligned}M_T(P^2,P'^2,P\cdot P')=&-\frac{1}{2\beta}\int k^2dk\int_0^{\pi}\sin\theta\,d\theta\\&\times\sum_{j=1}^{3}\frac{G(\vec{k},k_j^0)}{D_j(\vec{k},P,P')},\end{aligned} \tag{9.18}$$

where

$$G(\vec{k},k_j^0)=\frac{1}{2\pi^2}\sum_{i=0}^{3}a_i(k_c')z_i(P^2,P'^2,P\cdot P',\vec{k},k_j^0). \tag{9.19}$$

The $G(\vec{k},k_j^0)$ are the residues at the poles, with

$$k_1^0=E(\vec{k}), \tag{9.20}$$

$$k_2^0=E(\vec{k}+\vec{P})-P^0, \tag{9.21}$$

$$k_3^0=E(\vec{k}+\vec{P}')-P'^0. \tag{9.22}$$

The denominators are

$$D_1(\vec{k},\vec{P},\vec{P}',P^0,P'^0)=2E_q(\vec{k})[(E(\vec{k})+P^0)^2-E^2(\vec{k}+\vec{P})][(E(\vec{k})+P'^0)^2-E^2(\vec{k}+\vec{P}')], \tag{9.23}$$

$$D_2(\vec{k},\vec{P},\vec{P}',P^0,P'^0)=2E_q(\vec{k}+\vec{P})[(E(\vec{k}+\vec{P})-P^0)^2-E^2(\vec{k})][(E(\vec{k}+\vec{P})+P'^0-P^0)^2-E^2(\vec{k}+\vec{P}')], \tag{9.24}$$

and

$$D_3(\vec{k},\vec{P},\vec{P}',P^0,P'^0)=2E(\vec{k}+\vec{P}')[(E(\vec{k}+\vec{P}')-P'^0)^2-E^2(\vec{k})][(E(\vec{k}+\vec{P}')-P'^0+P^0)^2-E^2(\vec{k}+\vec{P})]. \tag{9.25}$$

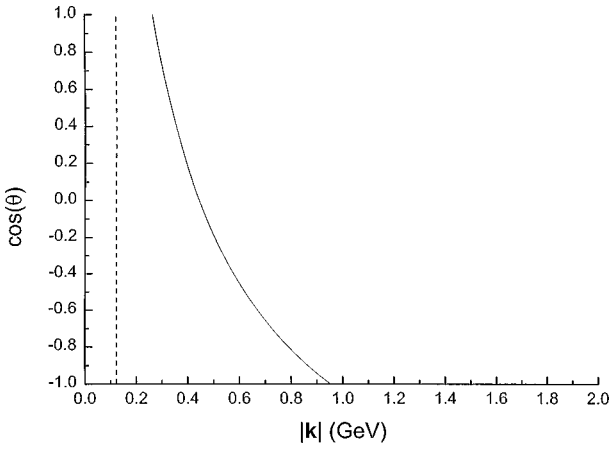

FIG. 17. The values of $\cos\theta$ and $|\vec{k}|$ that yield zeros of the denominator D_3, when the ρ is taken at rest, are shown as a dashed line, drawn at $|\vec{k}|=k_{\rm on}^{(\rho)}=[m_\rho^2/4-m^2]^{1/2}$. The solid line shows the zeros of D_2 that arise when $E_{\pi'}(\vec{P})=E(\vec{k}+\vec{P})+E(\vec{k})$. Here θ is the angle between $\vec{k}$ and $\vec{P}$.

Consider the evaluation of Eq. (9.18). If we put $\vec{P}=0$, θ is the angle between $\vec{k}$ and $\vec{P}'$, while, if $\vec{P}'=0$, θ is the angle between $\vec{k}$ and $\vec{P}$. For example, if $\vec{P}'=0$, the value of $|\vec{P}|$ is fixed by energy conservation. We exhibit the positions of the zeros of D_2 and D_3 for this case in Fig. 18. Note that D_3 is zero when $|\vec{k}|=k_{on}^{(\rho)}=(m_\rho^2/4-m^2)^{1/2}$, if the ρ is at rest. (See the dashed line in Fig. 17.) Further, D_2 is zero when values of θ and $|\vec{k}|$ lie on the curve in Fig 18 (solid line). (The zeros of D_3 correspond to ρ decay into a $q\bar{q}$ pair, while the zeros of D_2 correspond to the π' decay into a $q\bar{q}$ pair.)

X. CALCULATION OF THE AMPLITUDE FOR THE DECAY $\pi'\to\pi+\sigma$

The analysis is similar to that of the last section, except that the final state ρ is replaced by a σ. (Here the decay to $\pi+\sigma$ is meant to approximate three-pion decay, with two of the pions in a relative S state.) The analysis of experimental data for three-pion states is usually based upon this model in conjunction with the $\pi+\rho$ model of the last section. If the final pion has momentum $P-P'$ and the σ has momentum P', we have the amplitude

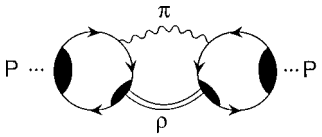

(a)

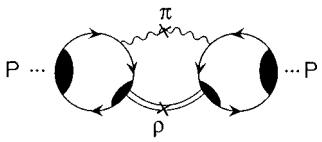

(b)

FIG. 18. (a) A contribution to the self-energy of a $q\bar{q}$ pseudoscalar excitation due to coupling to the $\pi+\rho$ channel is shown. The shaded areas denote the confinement vertex. [We neglect confinement for the $\pi(138)$.] This diagram serves to define the function $-iK_{\pi\rho}(P^2)$. (b) The imaginary part of $K_{\pi\rho}(P^2)$ may be obtained from the discontinuity of $K_{\pi\rho}(P^2)$ across the $\pi+\rho$ cut, when the π and ρ are on their (positive) mass shells. Note that we neglect π-ρ rescattering in the calculation of $K_{\pi\rho}(P^2)$.

$$M_{ij}=-2\delta_{ij}n_c\int\frac{d^4k}{(2\pi)^4}\,\mathrm{Tr}[\bar{\Gamma}_\sigma(P',k)S(P'+k)\gamma_5\times S(P+k)\bar{\Gamma}_5(P,k)S(k)],\tag{10.1}$$

where i,j are isospin indices. In Eq. (10.1) we have taken the final state pion to be emitted first. Also, in Eq. (10.1), $\bar{\Gamma}_\sigma(P',k)=c_0(P',k)+\hat{k}(P')c_1(P',k)$ and $\bar{\Gamma}_5(P,k)=\gamma_5[b_0(P,k)+\not{P}\,b_1(P,k)]$. When the σ is emitted first, the amplitude is

$$M'_{ij}=-2\delta_{ij}n_c\int\frac{d^4k}{(2\pi)^4}\,\mathrm{Tr}[\bar{\Gamma}_\sigma(P',k)S(k)\times\bar{\Gamma}_5(P,k)S(k-P)\gamma_5S(k-P')].\tag{10.2}$$

It is useful to write M'_{ij} as

$$M'_{ij}(P,P')=-2\delta_{ij}n_c\int\frac{d^4k}{(2\pi)^4}\,\mathrm{Tr}[\bar{\Gamma}_\sigma(P',k)S(k)\times\hat{\Gamma}_5(P,k)S(-(k+P))S(k+P')],\tag{10.3}$$

where we have introduced the notation $\bar{\Gamma}_5(P,k)=\gamma_5\hat{\Gamma}_5(P,k)$. We proceed to calculate

$$M_{ij,\,\rm tot}(P,P')=M_{ij}(P,P')+M'_{ij}(P,P')\tag{10.4}$$

and define $M_{ij,\,\rm tot}(P,P')=\delta_{ij}M_{\pi\sigma}(P,P')$. We find

$$M_{\pi\sigma}(P,P')=-n_cn_f\int\frac{d^4k}{(2\pi)^4}\,\frac{T(k,P,P')}{D(k)D(k+P)D(k+P')},\tag{10.5}$$

with $D(k)=(k^2-m^2+i\epsilon)$, etc. The function $T(k,P,P')$ is given by the following expressions:

$$T(k,P,P')=4[c_0(P',k)z_0(k,P,P')+c_1(P',k)z_1(k,P,P')],\tag{10.6}$$

with

$$z_0(k,P,P')=b_0(P,k)B_0^{(0)}(k,P,P')+b_1(P,k)B_1^{(0)}(k,P,P')\tag{10.7}$$

and

$$z_1(k,P,P')=b_0(P,k)B_0^{(1)}(k,P,P')+b_1(P,k)B_1^{(1)}(k,P,P').\tag{10.8}$$

Further,

$$B_0^{(0)}(k,P,P')=2m[m^2-(k+P)^2+P\cdot(P-P')],\tag{10.9}$$

TABLE II. Meson-quark coupling constants used in this work: $g_{\pi qq}$, $g_{\sigma qq}$, $g_{\rho qq}$.

	g	f_π (MeV)	Source
$\pi(138)$	3.93	92.6	Calculation with $m^0=0$ in the NJL model without confinement
$\sigma(600)$	3.00[a]		Ref. [3]
$\rho(770)$	3.93		Ref. [4]

[a]See the discussion in Sec. XI.

$$B_1^{(0)}(k,P,P')=2[(k^2+m^2)P\cdot(P'-P)+(m^2-k^2)P\cdot k-2(k\cdot P)(k\cdot P')-P^2k\cdot P'], \quad (10.10)$$

$$B_0^{(1)}(k,P,P')=2[\hat{k}^2(P')(m^2-(k+P)^2+P\cdot(P-P'))+\hat{k}(P')\cdot P(k^2+k\cdot P'-m^2)], \quad (10.11)$$

and

$$B_1^{(1)}(k,P,P')=2m[2\hat{k}^2(P')P\cdot(P'-P)+\hat{k}(P')\cdot P(m^2-k^2-2k\cdot P')]. \quad (10.12)$$

We now complete the integral in the complex k_0' plane to obtain

$$M_{\pi\sigma}(P,P')=n_c n_f(-i)\int\frac{d\vec{k}}{(2\pi)^3}\left[\frac{T_1(k,P,P')}{D_1}+\frac{T_2(k,P,P')}{D_2}+\frac{T_3(k,P,P')}{D_3}\right], \quad (10.13)$$

where $T_1(k,P,P')$ is $T(k,P,P')$ evaluated with $k^0_{(1)}=E(\vec{k})$, $T_2(k,P,P')$ is $T(k,P,P')$ evaluated with $k^0_{(2)}=E(\vec{k}+\vec{P}')-P'^0$ and $T_3(k,P,P')$ is $T(k,P,P')$ evaluated with $k^0_{(3)}=E(\vec{k}+\vec{P})-P^0$. (Note that $P'^0=[\vec{P}'^2+m_\sigma^2]^{1/2}$ and $P^0=[\vec{P}^2+m_{\pi'}^2]^{1/2}$.) In Eq. (10.13), the various denominators are

$$D_1=2E(\vec{k})[(E(\vec{k})+P^0)^2-E^2(\vec{k}+\vec{P})][(E(\vec{k})+P'^0)^2-E^2(\vec{k}+\vec{P}')], \quad (10.14)$$

$$D_2=2E(\vec{k}+\vec{P}')[(E(\vec{k}+\vec{P}')-P'^0)^2-E^2(\vec{k})]\times[(E(\vec{k}+\vec{P}')-P'^0-P^0)^2-E^2(\vec{k}+\vec{P})], \quad (10.15)$$

and

$$D_3=2E(\vec{k})[(E(\vec{k}+\vec{P})-P^0)^2-E^2(\vec{k})]\times[(E(\vec{k}+\vec{P})-P^0+P'^0)^2-E^2(\vec{k}+\vec{P}')]. \quad (10.16)$$

XI. CALCULATION OF THE WIDTHS

In this section we introduce the contribution to the self-energy of $q\bar{q}$ isovector pseudoscalar states due to the coupling to the $\pi+\rho$ or the $\sigma+\pi$ channel. (See Fig. 18.) We define a scalar function corresponding to the diagram shown in Fig. 18:

$$K_{\pi\rho}(P^2)=g_{\pi qq}^2g_{\rho qq}^2 2n_f^2n_c^2 i\int\frac{d^4P'}{(2\pi)^4}\times\frac{M_T^2(P^2,P'^2,P\cdot P')[P^2-(P\cdot P')^2/P'^2]}{[(P-P')^2-m_\pi^2+i\epsilon][P'^2-m_\rho^2+i\epsilon]}. \quad (11.1)$$

We may obtain $\mathrm{Im}\,K_{\pi\rho}(P^2)$ by calculating the discontinuity across the $\pi+\rho$ cut,

$$\mathrm{Im}\,K_{\pi\rho}(P^2)=\frac{1}{2}\mathrm{disc}K_{\pi\rho}(P^2), \quad (11.2)$$

and find, with $s=P^2$, $P'^2=m_\rho^2$, and $(P-P')^2=m_\pi^2$ that

$$\mathrm{Im}\,K_{\pi\rho}(s)=\frac{1}{64\pi}g_{\pi qq}^2g_{\rho qq}^2\frac{2n_f^2n_c^2}{m_\rho^2 s}M_T^2(s)\{[s-(m_\rho-m_\pi)^2]\times[s-(m_\rho+m_\pi)^2]\}^{3/2}. \quad (11.3)$$

If our states, π', are given a nonrelativistic normalization, $\langle\pi',\vec{P}'|\pi',\vec{P}\rangle=(2\pi)^3\delta(\vec{P}-\vec{P}')$, the relation between the width and $\mathrm{Im}\,K_{\pi\rho}$ is $\Gamma_{\pi\rho}=2\,\mathrm{Im}\,K_{\pi\rho}$.

Our result is obviously sensitive to the choice of $g_{\pi qq}$ and $g_{\rho qq}$. We use $m_q=0.364$ GeV and obtain a value for $g_{\pi qq}$ by working in the chiral limit. We find $g_{\pi qq}=3.93$ and $f_\pi=0.0926$ GeV, so that the Goldberger-Treiman relation, $m_q=g_{\pi qq}f_\pi$, is exactly satisfied. (For the final state pion, we use the physical mass of 138 MeV in the various kinematical relations.) Since, in our analysis, $g_{\rho qq}$ is momentum-dependent, we may write $g_{\rho qq}(P^2)$, with the relevant value for on-mass-shell ρ mesons being $g_{\rho qq}(m_\rho^2)$. In this work we use $g_{\rho qq}(m_\rho^2)=3.93$ which is the value we have calculated for Lorentz-vector confinement with $\kappa=0.0575\,\mathrm{GeV}^2$. (See Table II.)

A low-energy σ is often used in nuclear physics to represent correlated two-pion exchange. Also, three-pion final states are often represented by $\pi+\rho$ and $\pi+\sigma$ configurations (Fig. 10). If we accept the $\pi+\sigma$ model for the three-pion final state with one pion pair coupled to $L=0$, we need to calculate $K_{\pi\sigma}(P^2)$, which is the analog of $K_{\pi\rho}(P^2)$ shown in Fig. 18.

For the $\pi+\sigma$ intermediate state in Fig. 18, we find

TABLE III. Calculated widths of pseudoscalar states for decay into the $\pi+\sigma$ and $\pi+\rho$ channels are given. The states at 1.47, 1.63, and 1.68 GeV have very small widths and are not listed.

Energy (GeV)	$\Gamma_{\pi\sigma}$ (MeV)	$\Gamma_{\pi\rho}$ (MeV)	$\Gamma_{\rm tot}$ (MeV)
1.18	58	310	368
1.36	31	119	150

$$\mathrm{Im}\,K_{\pi\sigma}(s)=\frac{g^2_{\sigma qq}g^2_{\pi qq}}{16\pi s}\times\sqrt{(s-(m_\sigma-m_\pi)^2)(s-(m_\sigma+m_\pi)^2)}\times|M_{\sigma\pi}(s)|^2 \tag{11.4}$$

with $\Gamma_{\sigma\pi}/2=\mathrm{Im}\,K_{\pi\sigma}(m^2_{\pi'})$, if the π' state is given a nonrelativistic normalization, $\langle\pi',\vec{P}'|\pi',\vec{P}\rangle=(2\pi)^3\delta^{(3)}(\vec{P}-\vec{P}')$. Here we need to make a choice for $g_{\sigma qq}(m^2_\sigma)$. We have made an extensive study of scalar-isoscalar $q\bar{q}$ states in Ref. [3], where we also included singlet-octet mixing. In Ref. [3], a study of the quark-quark interaction led to the estimate $g_{\sigma qq}(0)=3.32$. That value was generally in accord with a quark model we developed for the description of scalar-isoscalar exchange in the one-boson exchange model of the nucleon-nucleon force. (See the first item in Ref. [2] and Ref. [3].) Since we expect some variation as we go from $g_{\sigma qq}(0)$ to $g_{\sigma qq}(m^2_\sigma)$, we take $g_{\sigma qq}(m^2_\sigma)=3.00$. There is, at least, a 10% theoretical uncertainty in this value, beyond whatever limitation exists for the $\pi+\sigma$ description of the final three-pion state.

The widths calculated with the parameters mentioned above are given in Table III. The results given there are used to generate the solid curves in Figs. 19 and 20. To construct Figs. 19 and 20, we have used only the state at 1.18 GeV.

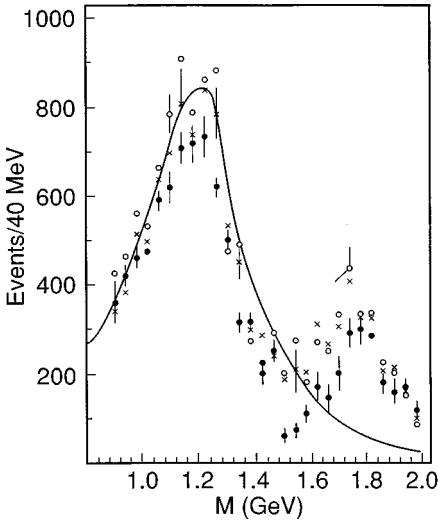

FIG. 19. Data taken from Ref. [8] are shown. The figure shows the member of events (taken in 40 MeV intervals) corresponding to the decay $\pi'\to\pi+(\pi+\pi)_{L=0}$. The various data sets shown correspond to the different theoretical schemes used to analyze the data. The solid line shows the squared T matrix of our state at 1.18 GeV (in arbitrary units).

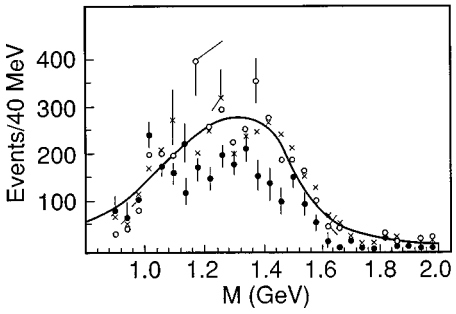

FIG. 20. The figure shows the number of events (taken at 40 MeV intervals) corresponding to the decay $\pi'\to\pi+(\pi+\pi)_{L=1}$ or $\pi'\to\pi+\rho$. The solid curve represents the squared T matrix for our state at 1.18 GeV presented with an arbitrary normalization.

Here we have assumed that the state at 1.36 GeV is only weakly excited in the reaction that creates the three-pion final state.

XII. DISCUSSION AND CONCLUSIONS

We may consider the following interpretation of our results. We start with the observation that, if $G_S=G_V=0$, the potential $V^C(\vec{k}-\vec{k}')$ acts and provides doublets at $P^0=1.20$, 1.49, and 1.69 GeV. These states give rise to the singularities of Γ^{+-}_5 and Γ^{+-}_L seen in the values of $J^{PP}(P^2)$, $J^{PA}(P^2)$, and $J^{AA}(P^2)$. (See Figs. 9–11.) One member of the doublet is a pseudoscalar state and the other is a (longitudinal) axial-vector state. When we turn on the NJL interaction, the degeneracy is lifted. In large part, the $1S$ pseudoscalar state becomes the pion, moving down over 1 GeV from $P^0=1.20\,\mathrm{GeV}$ to $P^0=0.138\,\mathrm{GeV}$. The axial-vector state is mixed with the pseudoscalar state and the mixed state is at 1.18 GeV, quite close to 1.20 GeV, the original position of the $1S$ states. (See Fig. 15.)

We next consider the $2S$ states that were at 1.49 GeV, when $G_S=G_V=0$. With reference to Table I and Fig. 15, we see that there is a state at $P^0=1.36\,\mathrm{GeV}$ which gives rise to a resonance seen in T_2. That state may be identified as the $\pi(2S)$ state. The next (mixed) state is at 1.47 GeV, indicating almost no downward movement from the original position at 1.49 GeV.

Finally, we consider the $3S$ states, which are at 1.69 GeV when $G_S=G_V=0$. These states evolve into our states at 1.68 and 1.63 GeV. The latter state may be classed as ''pionlike,'' since it appears as a resonance in T_1 and has a small mixing angle. The other (mixed) state has only moved down about 10 MeV from the original position at 1.69 GeV. This analysis suggests, therefore, that the $\pi(3S)$ is the state we obtained at 1.63 GeV.

The information concerning states in the intermediate-energy range above 1 GeV is largely obtained through the study of three-pion final states [8,9]. For states with the quantum numbers of the pion, we only find the $\pi(1300)$ below 1.7 GeV in the data tables [7]. Our analysis suggests the presence of a total of six states with masses less than 1.7 GeV. We have found that the nodeless state at 1.18 GeV and the state at 1.36 GeV have significant widths for the decays $\pi'\to\pi+\sigma$ and $\pi'\to\pi+\rho$. Our model gives a good fit to the position of the peak seen in the data shown in Fig. 19 if

we assume the state at 1.36 GeV is weakly excited in the reaction leading to the three-pion final state.

When we consider the decay $\pi' \to \pi + \rho$, we find that the 1.18 GeV state and the 1.36 GeV have large widths, while the other states have quite small widths. When theoretical analysis is used to extract the decays of the nature $\pi' \to \pi + \rho$ from experimental data for the three-pion final state, the results are rather model dependent and the values shown in Fig. 20 exhibit significant scatter. For Fig. 20 we again limit ourselves to the state at 1.18 GeV in creating the figure. (Our theoretical curve is given an arbitrary normalization.) We should keep in mind that we are not fitting experimental data, but are fitting ''data'' extracted using a simple theory of the final-state dynamics. The fact that we do not obtain a good result for the branching ratio suggests that a study of final-state interactions in the (coupled) $\pi+\rho$ and $\sigma+\pi$ channels may be necessary to obtain both the cross section and branching ratio. Such a study is beyond the scope of this work.

As a final point, we remark that the $\pi(1800)$ that appears in the data shown in Fig. 19 is unlikely to be a $q\bar{q}$ state, since $q\bar{q}$ states with several nodes have very small widths in our model. (In our analysis, a state at 1.8 GeV would have at least three nodes in its wave function.)

ACKNOWLEDGMENTS

This work was supported in part by a grant from the National Science Foundation and by the PSC-CUNY Faculty Research Award Program.

APPENDIX A

In this appendix we present the equations that we have solved to obtain γ_1^{+-}, γ_2^{+-}, etc. We have, with $k=|\vec{k}|$, $k'=|\vec{k}'|$ and $x=\cos\theta$, where θ is the angle between $\vec{k}$ and $\vec{k}'$,

$$\gamma_1^{+-}(P^0,k)=1+\int \frac{d^3k'}{(2\pi)^3}\left[\left(\frac{2k'^2x}{E^2(k')}+\frac{k'}{k}\frac{m^2x^2}{E^2(k')}\right)\frac{k}{k'}\frac{\gamma_1^{+-}(P^0,k')}{P^0-2E(k')}+(1-x^2)\frac{\gamma_2^{+-}(P^0,k')}{P^0-2E(k')}\right]V^C(\vec{k}-\vec{k}') \tag{A1}$$

and

$$\gamma_2^{+-}(P^0,k)=1-\int \frac{d^3k'}{(2\pi)^3}\left[\frac{-m^2}{2E^2(k')}(1-x^2)\frac{\gamma_1^{+-}(P^0,k')}{P^0-2E(k')}-\left(\frac{(1+x^2)}{2}+\frac{kk'x}{E(k)E(k')}\right)\frac{\gamma_2^{+-}(P^0,k')}{P^0-2E(k')}\right]\times V^C(\vec{k}-\vec{k}'). \tag{A2}$$

We find that $\gamma_1^{-+}=\gamma_1^{+-}$ and γ_2^{-+} satisfies the equation

$$\gamma_2^{-+}(P^0,k)=1-\int \frac{d^3k'}{(2\pi)^3}\left[\frac{m^2}{2E^2(k')}(1-x^2)\frac{\gamma_1^{+-}(P^0,k')}{P^0+2E(k')}+\left(\frac{(1+x^2)}{2}+\frac{kk'x}{E(k)E(k')}\right)\frac{\gamma_2^{-+}(P^0,k')}{P^0+2E(k')}\right]\times V^C(\vec{k}-\vec{k}'), \tag{A3}$$

where we have inserted γ_1^{+-} for γ_1^{-+} in the first term of the large bracket.

Once we have calculated γ_1^{+-}, γ_2^{+-}, and γ_2^{-+}, we can obtain γ_1^{++} from the relation

$$\gamma_1^{++}(P^0,k)=1-\int \frac{d^3k'}{(2\pi)^3}V^C(\vec{k}-\vec{k}')\left[\frac{4m^2}{E^2(k')}\times\left(\frac{2xk'}{k}-x^2\right)\frac{\gamma_1^{+-}(P^0,k')}{(P^0)^2-4E^2(k')}-(1-x^2)\times\left(\frac{\gamma_2^{+-}(P^0,k')}{P^0-2E(k')}-\frac{\gamma_2^{-+}(P^0,k')}{P^0+2E(k')}\right)\right]. \tag{A4}$$

Using Eqs. (A1)–(A4), we obtain

$$a_0=\frac{mk}{E^2(k)}[-\gamma_1^{+-}+\gamma_1^{++}], \tag{A5}$$

$$a_1=-\frac{m^2}{E^2(k)}\left[\gamma_1^{+-}+\frac{k^2}{m^2}\gamma_1^{++}\right], \tag{A6}$$

$$a_2=\frac{1}{2}[\gamma_2^{+-}+\gamma_2^{-+}], \tag{A7}$$

and

$$a_3=\frac{E(k)}{2k}[\gamma_2^{-+}-\gamma_2^{+-}]. \tag{A8}$$

We see that we need not calculate γ_2^{++}, γ_1^{--}, or γ_2^{--} to obtain the a_i $(i=0,1,2,3)$. We record the relation between the γ_i and Γ's: $\gamma_1^{+-}=(-k/m)\Gamma_1^{+-}$, $\gamma_2^{+-}=\Gamma_2^{+-}$, $\gamma_1^{-+}=\gamma_1^{+-}$, $\gamma_2^{-+}=\Gamma_2^{-+}$, $\gamma_1^{++}=(m/k)\Gamma_1^{++}$, $\gamma_2^{++}=\Gamma_2^{++}$, $\gamma_1^{--}=(m/k)\Gamma_1^{--}$, and $\gamma_2^{--}=\Gamma_2^{--}$.

[1] For reviews of the NJL model, see T. Hadsuda and T. Kinihiro, Phys. Rep. **247**, 223 (1994); U. Vogl and W. Weise, Prog. Part. Nucl. Phys. **27**, 195 (1991); S. P. Klevansky, Rev. Mod. Phys. **64**, 649 (1992).

[2] L. S. Celenza, Xiang-Dong Li, and C. M. Shakin, Phys. Rev. C **55**, 3083 (1997); L. S. Celenza, C. M. Shakin, Wei-Dong Sun, J. Szweda, and Xiquan Zhu, Phys. Rev. D **51**, 3638 (1995).

[3] L. S. Celenza, Xiang-Dong Li, and C. M. Shakin, Phys. Rev. C **56**, 3326 (1997).

[4] Bo Huang, Xiang-Dong Li, and C. M. Shakin, Phys. Rev. C **58**, 3648 (1998).

[5] L. S. Celenza, Bo Huang, and C. M. Shakin, Brooklyn College Report No. BCCNT 97/091/266 (1997) (unpublished).

[6] L. S. Celenza, Xiang-Dong Li, and C. M. Shakin, Phys. Rev. C **55**, 1492 (1997).

[7] Particle Data Group, R. M. Barnett *et al.*, Phys. Rev. D **54**, 1 (1996). This reference contains a comprehensive survey of elementary particle properties.

[8] G. Bellini *et al.*, Phys. Rev. Lett. **48**, 1697 (1982).

[9] See, for example, G. Bellini *et al.*, Phys. Rev. Lett. **48**, 1697 (1982); R. Aron and R. S. Longacre, Phys. Rev. D **24**, 1207 (1981); M. Zielinski *et al.*, *ibid.* **30**, 1855 (1984).